ACS OMEGA

Open Access

http://pubs.acs.org/journal/acsodf

Article

Composite Hydrogel of Poly(vinyl alcohol) Loaded by *Citrus hystrix* Leaf Extract, Chitosan, and Sodium Alginate with In Vitro Antibacterial and Release Test

Kusjuriansah Kusjuriansah, Marathur Rodhiyah, Nabila Asy Syifa, Halida Rahmi Luthfianti, William Xaveriano Waresindo, Dian Ahmad Hapidin, Tri Suciati, Dhewa Edikresnha, and Khairurrijal Khairurrijal*

Cite This: *ACS Omega* 2024, 9, 13306−13322

Read Online

ACCESS | Metrics & More | Article Recommendations | Supporting Information

ABSTRACT: *Citrus hystrix* leaves have been used traditionally as a spice, a traditional medicine for respiratory and digestive disorders, and a remedy for bacterial infections. This study reports on the synthesis of composite hydrogels using the freeze−thaw method with poly(vinyl alcohol) (PVA) as the building block loaded by *C. hystrix* leaf extract (CHLE). Additionally, chitosan (CS) and sodium alginate (SA) were also loaded, respectively, to increase the antibacterial activity and to control the extract release of the composite hydrogels. The combinations of the compositions were PVA, PVA/CHLE, PVA/CHLE/CS, PVA/CHLE/SA, and PVA/CHLE/SA/CS. The internal morphology of the hydrogels shows some changes after the PVA/CHLE hydrogel was loaded by CS, SA, and SA/CS. The analysis of the Fourier transform infrared (FTIR) spectra confirmed the presence of PVA, CHLE, CS, and SA in the composite hydrogels. From the X-ray diffraction (XRD) characterization, it was shown that the composite hydrogels maintained their semicrystalline properties with decreasing crystallinity degree after being loaded by CS, SA, and SA/CS, as also supported by differential scanning calorimetry (DSC) characterization. The compressive strength of the PVA/CHLE hydrogel decreases after the loading of CS, SA, and SA/CS, so that it becomes more elastic. Despite being loaded in the composite hydrogels, the CHLE retained its antibacterial activity, as evidenced in the in vitro antibacterial test. The loading of CS succeeded in increasing the antibacterial activity of the composite hydrogels, while the loading of SA resulted in the decrease of the antibacterial activity. The release of extract from the composite hydrogels was successfully slowed down after the loading of CS, SA, and SA/CS, resulting in a controlled release following the pseudo-Fickian diffusion. The cytotoxic activity test proved that all hydrogel samples can be used safely on normal cells up to concentrations above 1000 μg/mL.

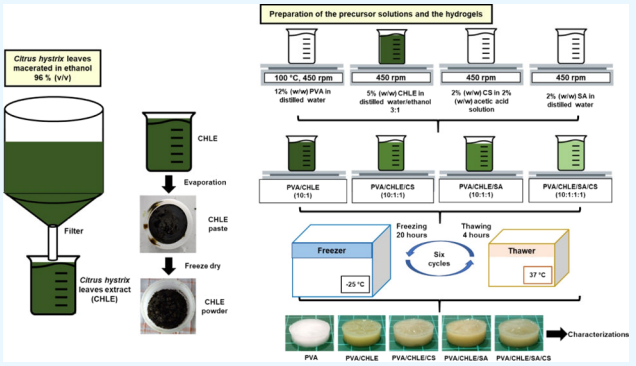

1. INTRODUCTION

Citrus hystrix leaves have been used traditionally as a spice in food and a traditional medicine for respiratory and digestive disorders and bacterial infections.[1] Through phytochemical analysis, *C. hystrix* leaves are confirmed to contain several chemical compounds, such as alkaloids, flavonoids, tannins, terpenoids, quinones, proteins, carbohydrates, and glycosides.[2] From the gas chromatography−mass spectrometry (GC−MS) analysis, it is proven that the essential oil extracted from *C. hystrix* leaves consists of several important chemical compounds, such as citronellal (80.04%), citronellol acetate (5.46%), β-citronellol (4.13%), linalool (3.04%), and other chemical compounds.[3] *C. hystrix* leaves are proven to inhibit bacterial growth from 411 isolates of groups A, B, C, F, and G Streptococci, *Streptococcus pneumoniae*, *Haemophilus influenzae*, *Staphylococcus aureus*, and *Acinetobacter baumannii*. The antibacterial activity of *C. hystrix* leaves is due to the presence of citronellal, the main compound inside the leaves which acts as the antibacterial agent.[4] In general, the application of an antibacterial agent requires a medium of delivery. Currently, hydrogels are being massively used and researched for drug delivery with loaded antibacterial agents.

A hydrogel is a soft material in the form of a three-dimensional network that is able to absorb a certain amount of liquid.[5] The synthesis of the hydrogel involved polymers, whether natural, synthetic, or a mixture of both.[6] Natural polymers are biocompatible and biodegradable and possess

Received: December 19, 2023
Revised: January 30, 2024
Accepted: February 20, 2024
Published: March 5, 2024

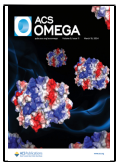

https://doi.org/10.1021/acsomega.3c10143
ACS Omega 2024, 9, 13306−13322

good biological activity. However, they usually have weak mechanical properties.[7] Some examples of natural polymers that have been used as hydrogel matrices are alginate[8] and chitosan (CS).[9] On the other hand, synthetic polymers generally have strong mechanical properties but usually poor biological activity.[10] An example of synthetic polymers that have been used to synthesize hydrogels is poly(vinyl alcohol) (PVA).[11] PVA is soluble in water, and it can be used to form a hydrogel by means of the freeze−thaw technique.[12] PVA hydrogels have superior characteristics, such as being biocompatible and biodegradable and possessing strong mechanical properties.[13] PVA can also be combined with natural polymers to improve the performance of the hydrogel. Sodium alginate (SA) is a natural polymer with a large water absorption capacity.[14] The blending of SA with PVA resulted in a PVA/SA hydrogel having strong mechanical properties and high water absorption.[15] To enhance the capabilities of the hydrogels, chitosan can also be added. Chitosan is a natural polymer with a significant intrinsic antibacterial capacity.[16] The loading of CS in the PVA hydrogel then forms a PVA/CS hydrogel, which has strong mechanical properties and antibacterial activity.[17] SA and CS can also be combined simultaneously with PVA, resulting in a hydrogel with strong mechanical properties, high water absorption, and antibacterial activity.[18]

During the synthesis of the hydrogel, cross-links between polymer chains are formed.[19] Freeze−thaw is one of the straightforward and inexpensive physical cross-linking methods that result in a hydrogel.[20] In previous studies, the PVA hydrogel has been researched to be delivery medium for antibacterial agents from the extracts of red betel and guava leaves. The antibacterial activity test showed that the composite hydrogel had the antibacterial activity derived from the loading of the extract.[20,21] In another study, a PVA hydrogel loaded with CS was used as delivery medium for honey and allantoin as a wound dressing. The release test showed that the release of allantoin from the hydrogel occurred also following the Fickian diffusion model.[22] In the other experiment, the PVA/SA hydrogel synthesized by using a freeze−thaw method has also been used as delivery medium for ampicillin as the antibiotic agent. The release test showed that the loading of SA in the PVA hydrogel reduced the release rate of ampicillin and resulted in a controlled release.[23] Lastly, the PVA hydrogel loaded with SA/CS has been used as delivery medium for Ag@MOF-loaded CS nanoparticles. The result of the in vivo test on rats showed that the hydrogel can accelerate wound healing and re-epithelialization.[24] From this study, it is proven that the antibacterial agents loaded in the PVA/SA/CS hydrogels synthesized from PVA, SA, and CS do not lose their antibacterial activity. Therefore, composite hydrogels can potentially be used as a wound dressing.

Based on the described references, it is expected that the hydrogel synthesized from the blending of PVA, SA, and CS can be used as delivery medium for *C. hystrix* leaf extract (CHLE), which acts as the antibacterial agent. Although there are many studies regarding the CHLE, no study has been conducted regarding the use of a hydrogel as the delivery medium for CHLE. Therefore, this study aims to develop and characterize composite hydrogels from PVA, SA, CS, and CHLE synthesized by freeze−thaw. The composite hydrogels were characterized both physically and microbiologically. Physical characterizations included the following: scanning electron microscopy (SEM), Fourier transform infrared (FTIR), X-ray diffraction (XRD), thermogravimetry analysis (TGA), differential scanning calorimetry (DSC), gel fraction, texture profile analysis (TPA), and compression test. Meanwhile, microbiological characterizations were conducted with the in vitro antibacterial activity test, release test, and cytotoxic activity.

2. RESEARCH METHODS

2.1. Materials. The 99% hydrolyzed PVA with a molecular weight of 89,000−98,000 g/mol was obtained from Sigma-Aldrich. SA with 99% purity and CS in the powder form were purchased from Chimultiguna Indramayu, Indonesia. The molecular weight and deacetylation degree of CS were 153,000 g/mol and 95.22%, respectively. The analytical grade ethanol was obtained from Merck, Germany. The deionized water was obtained from the ITB Department of Chemistry ITB. *C. hystrix* leaves were obtained from Sumedang, West Java, Indonesia.

2.2. Preparation of *C. hystrix* Leaf Extract and the Hydrogels. *C. hystrix* leaf extract (CHLE) was produced as follows. *C. hystrix* leaves were first crushed into powder using a blender. The powder was then extracted by maceration in 96% (v/v) ethanol for 3 days. The resulting extract was then evaporated at a temperature of 50 °C using a rotary evaporator to obtain the extract in the form of a paste. Prior to use in the synthesis of hydrogels, the paste was dried into a powder form using a freeze dryer (Eyela, FD-5N). The extraction method is similar to the previous study with slight modifications.[25] CHLE solution was made in a concentration of 5% w/w by dissolving the CHLE powder into the solution system consisting of distilled water and ethanol with a weight ratio of 3:1 and then stirred using a magnetic stirrer until homogeneously mixed. The 12% w/w PVA solution was prepared by dissolving PVA powder into distilled water and then stirred using a magnetic stirrer at a temperature of 100 °C for 3 h. CS solution was made by dissolving CS powder at a concentration of 2 wt % in a 2% (w/w) acetic acid solution. The solution was then stirred using a magnetic stirrer until it was homogeneous. The SA solution was prepared by dissolving 2% w/w SA powder in distilled water.

The PVA solution was then mixed with the CHLE solution in a weight ratio of PVA/CHLE = 10:1. After that, for every 11 g of the PVA/CHLE solution, 1 g of the CS solution was added to produce a PVA/CHLE/CS solution or 1 g of the SA solution was added to give PVA/CHLE/SA solution. The PVA/CHLE/SA/CS solution was then prepared by adding 1 g of the SA solution and 1 g of the CS solution into the PVA/CHLE solution. The PVA solution was also included as the pure PVA hydrogel, which was also studied to observe any difference in the characteristics of hydrogels as more substances are added. Thus, there were five precursor solutions prepared, namely, PVA, PVA/CHLE, PVA/CHLE/CS, PVA/CHLE/SA, and PVA/CHLE/SA/CS. Each precursor solution was then placed in a tubular pot zalp with a volume of about 12 mL. The solution was then placed in an ultrasonic bath to remove bubbles. The freeze−thaw process consisted of six cycles, with 20 h of freezing and 4 h of thawing. The freezing was carried out at a temperature of −25 °C, while the thawing was carried out at a temperature of 37 °C. The synthesis method followed the previous research with slight modifications.[20,21] Before further characterization, the hydrogel was then dried at 50 °C in an oven until the mass was constant to remove the liquid phase.

https://doi.org/10.1021/acsomega.3c10143
ACS Omega 2024, 9, 13306−13322

2.3. Physicochemical Characterizations of Hydrogels. The internal hydrogel morphology was observed using a SEM (JEOL, JSM-6360 LA) with an excitation voltage of 15 kV and magnifications of 1000× and 5000×. The as-formed hydrogel was initially freeze-dried and then cut in a plane parallel to the cylinder axis.[20] The identification of functional groups and intermolecular interactions in powder samples and hydrogel samples was carried out using FTIR (Bruker, Alpha Platinum ATR A220/D-01), in the range of wavenumbers from 500 to 4500 cm^{-1}. The crystallinity of powder samples and hydrogel samples was identified using XRD (Rigaku, SmartLab, Japan), with a Cu (Kα) irradiation source, operating voltage of 40 kV, electric current of 30 mA, and wavelength of 1.5405 Å. The thermal characterization was carried out to identify the thermal stability of the powder samples and hydrogel samples. The measurements were carried out under ordinary environmental conditions, a temperature range of 30−600 °C, and a heating rate of 10 °C/min, by placing the samples on aluminum pans in thermogravimetry and differential thermal analysis (TG/DTA) (STA7300, Hitachi). The gel fraction of the hydrogels was studied by immersing the dried hydrogel in a pot zalp filled with phosphate buffer saline (PBS) with pH 7.4 and at a temperature of 37 °C until 48 h. After that, the hydrogel was dried again, until the mass was constant. The gel fraction is defined as the ratio of hydrogel mass after redrying (w_3) to hydrogel mass before immersion (w_1), as presented in eq 2[20]

$$\text{gel fraction (\%)} = \frac{w_3}{w_1} \times 100\% \quad (1)$$

The hydrogel texture was analyzed using the texture profile analysis (TPA) method using a Texture Analyzer TXT 32. Hydrogel samples were prepared in a cylindrical shape with diameters of 20−22 mm and thicknesses of 4−6 mm. TPA was used to measure the mechanical resistance of the hydrogel samples to probe penetration. The parameters observed include hardness, adhesiveness, springiness, cohesiveness, gumminess, chewiness, and resilience. The compressive strength of the hydrogel was measured using a universal tensile machine (UTM) (Sinowon SM-200) with a strain rate of 10 mm/min. The hydrogel was first prepared in the form of a cylinder with a diameter of about 20−22 mm and a thickness of about 4−6 mm.

2.4. In Vitro Antibacterial Test. The antibacterial activity of the hydrogel was identified using the agar diffusion method, as was done in the previous study.[20,21] The bacteria used were *S. aureus* (ATCC 6538) as Gram-positive bacteria and *Pseudomonas aeruginosa* (ATCC 9027) as Gram-negative bacteria. The as-formed hydrogel was first prepared with a thickness of about 5 mm and diameter of about 23 mm. The mass of the hydrogel was weighed and sterilized for 20 min using UV light. Petri dishes containing Mueller−Hinton agar (MHA) media as the bottom agar were then prepared. The hydrogel was placed in the MHA media. The top agar consisting of MHA media and bacteria was then poured over the hydrogel and leveled to cover the surface of the bottom agar. The agar with bacteria but without any hydrogel was also prepared to be used as the control variable. The samples were then incubated at 37 °C for 24 h. After incubation, the zone of inhibition of the bacteria appeared and can then be measured. Afterward, 50 μL of top agar in the zone of inhibition was taken and diluted into NaCl solution with varying concentrations. A 500 μL aliquot of NaCl solution with diluted agar was then swabbed onto a Petri dish until evenly distributed over the entire surface. The samples were then incubated at 37 °C for 24 h. The number of bacterial colonies that grew was counted to determine the antibacterial activity of the hydrogel. The antibacterial activity was calculated using eq 1[20]

$$\text{antibacterial activity} = \frac{[(\log \text{control (cfu·mL}^{-1})) - (\log \text{hydrogel (cfu·mL}^{-1}))]}{\text{mass (g)}\cdot(\log \text{control (cfu. mL}^{-1}))} \quad (2)$$

2.5. Release Test. The release test was carried out to identify the ability of the hydrogel to release the loaded CHLE. CHLE was first calibrated using a UV−vis spectrophotometer (Beckman Coulter, DU 7500i). CHLE was dissolved in the system of ethanol−water solvent with a ratio of 1:3 (w/w), and then, the absorbance peak was obtained at a wavelength of 205 nm. The calibration results are graphed to obtain the relationship between the CHLE concentration and the absorbance. The release test was started by immersing the hydrogel in PBS solution (pH 7.4) at a volume of 400 mL. The test was carried out using a paddle dissolution (Hanson Research, SR8 Plus), within 3 h, at a temperature of 37 °C and a rotational speed of 50 rpm. For every 20 min, the PBS solution with a volume of 5 mL was taken and replaced with a new PBS solution with the same volume. The solution was then measured for absorbance so that the concentration of CHLE released could be determined. The procedure was in accordance with previous research.[20]

2.6. Cytotoxic Activity. The cytotoxic test of the hydrogel samples was carried out using the Presto Blue test, as was done in the previous study.[26] Cell viability was then measured using the Presto Blue reagent obtained from Thermofisher A13262. The reagent can evaluate various cells based on the resazurin compound. The reduction ability of living cells is then used to quantitatively determine the proliferation rate of the sample. These results show that healthy cells will experience a reduction in the level of their cytoplasm. The reduction of resazurin as a nonfluorescent blue dye to resorufin as a pink fluorescent dye then becomes an indicator of cell viability. The number of active cells is then indicated through the conversion. Normal cells (CV-1) were cultured until the cell growth percentage reached 70% and then diluted using complete Roswell Park Memorial Institute (RPMI) liquid culture medium. Then, the final cell density of 17,000 cells/well was used in 96-well plates with samples to be incubated for 24 h at 37 °C and 5% CO_2 gas.

The samples were then diluted into eight concentration variants in PBS and dimethyl sulfoxide (DMSO), namely, 7.81, 15.63, 31.25, 62.50, 125.00, 250.00, 500.00, and 1000.00 μg/mL. The positive control used in this test is cisplatin. All samples were then incubated again for 48 h. After that, the medium was prepared in 10 μL of Presto Blue reagent and 90 μL of RPMI medium. The mixture was then put into each well plate and then incubated for 1−2 h until a color change was seen. The color change occurs from the blue resazurin compound with no intrinsic fluorescence value to the resazurin compound which is pink and very fluorescent. Next, the absorbance was measured at wavelengths of 570 and 600 nm using a multimode reader. The IC_{50} value was then calculated from the concentration required to inhibit growth by 50%. This concentration is obtained from the graph of cytotoxicity against the sample concentration. Each test and analysis were carried out twice, and the results were averaged.

https://doi.org/10.1021/acsomega.3c10143
ACS Omega 2024, 9, 13306−13322

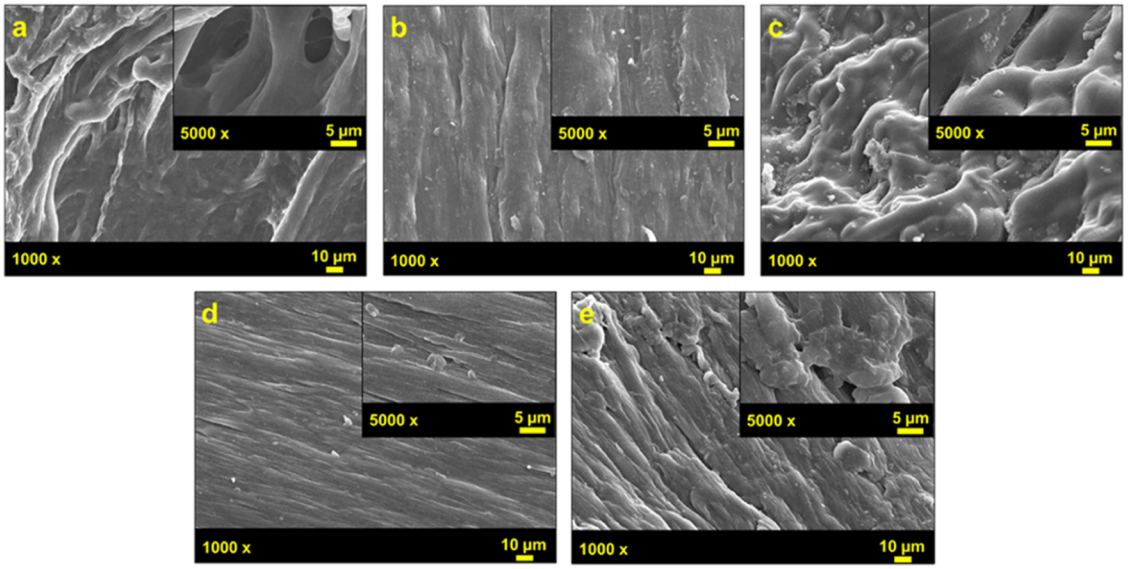

Figure 1. SEM images of (a) PVA, (b) PVA/CHLE, (c) PVA/CHLE/CS, (d) PVA/CHLE/SA, and (e) PVA/CHLE/SA/CS hydrogels.

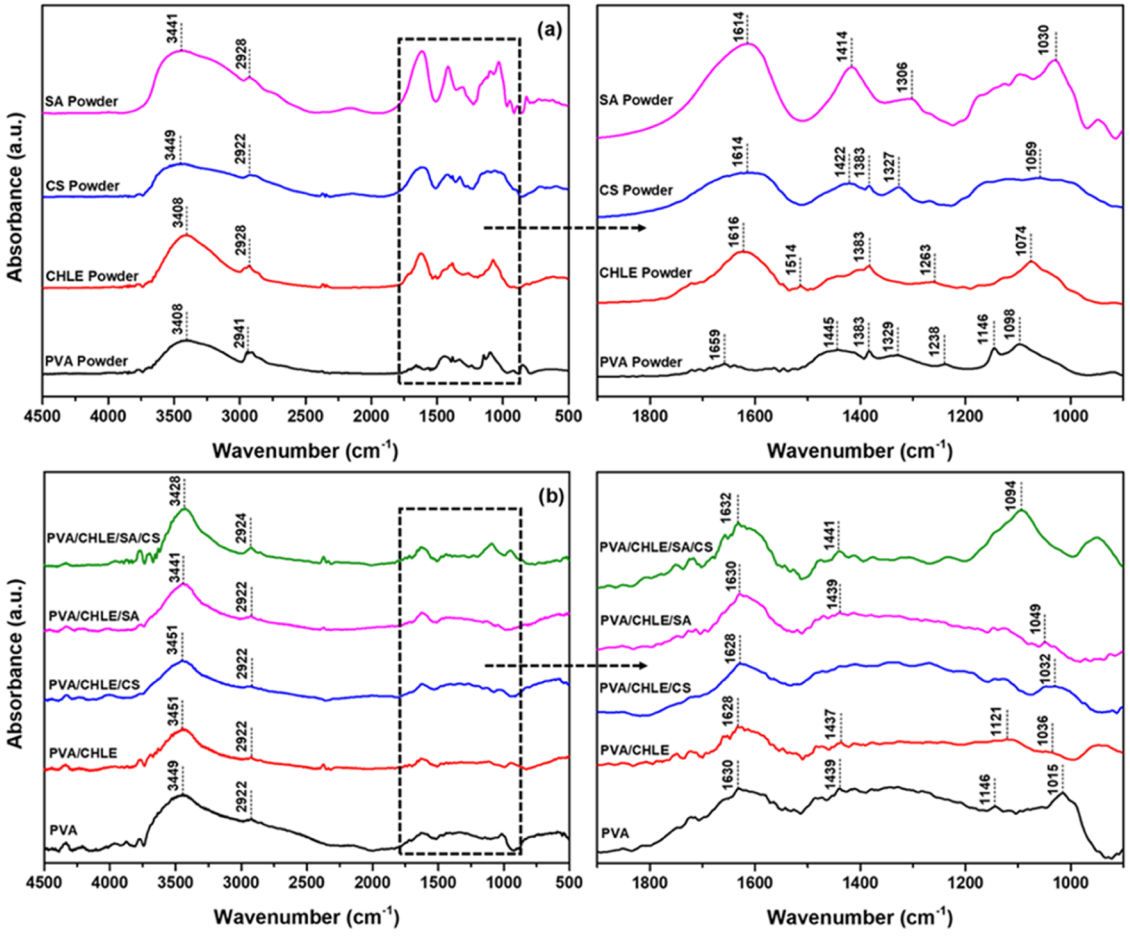

Figure 2. FTIR spectra of (a) powder samples and (b) hydrogel samples.

2.7. Statistical Analysis. Measurement of release was carried out three times. For the antibacterial activity test, there were two samples (n = 2) for each composite hydrogel combination. Statistical analysis applied was one-way analysis of variance (ANOVA) and Tukey's honestly significant difference (HSD) post hoc test. The analysis was carried out using IBM SPSS 24 software at a confidence level of more than 95% ($p < 0.05$).[21] Different superscript letters indicate significant differences between measurement results ($p < 0.05$).

https://doi.org/10.1021/acsomega.3c10143
ACS Omega 2024, 9, 13306−13322

3. RESULTS AND DISCUSSION

3.1. SEM Images. The SEM images of the hydrogels are presented in Figure 1. The PVA hydrogel exhibits a porous morphology. A similar morphology was also found in the previous study,[27] where the intratubule and intertubule cross-linked PVA tubules led to the formation of the identical morphology. The loading of CHLE in the PVA hydrogel resulted in a morphological change from porous to nonporous. The CHLE is known to contain many active substances, such as polysaccharides, which can penetrate into the free space between PVA cross-links so that it becomes more relaxed and closes the pores of the hydrogel.[2,28] These polysaccharides are known to have antibacterial activity by blocking carbohydrate receptors involved in host−bacterial interaction.[29] The ethanolic CHLE has less solubility in water compared to PVA in water, which forces the CHLE to agglomerate like a cube, as a result of different solubility repulsion.[30] These results proved the presence of CHLE in the hydrogel that has antibacterial activity,[3] as confirmed by the result of the antibacterial activity test.

The SEM image of the PVA/CHLE/CS hydrogel revealed a cross-linked network and a porous morphology, which further predisposed the extract release to be prolonged, as confirmed by the result of the release test.[31] These morphological changes are caused by the interaction between the CS and PVA functional groups, which formed hydrogen bonding, as also found in previous studies.[31,32] For the PVA/CHLE/SA hydrogel, the morphology of the hydrogel showed very tiny pores due to differences in the degree of homogeneity, hydrophilicity, or miscibility between SA and PVA, as also found in the previous study.[23] This morphology was responsible for reducing the extract release, as confirmed by the result of the release test. Lastly, the loading of SA and CS in the PVA/CHLE hydrogel resulted in morphological changes that appeared to be a combination of the loading effects of SA and CS, as previously described.

3.2. FTIR Spectra. The FTIR spectra of the powder and hydrogel samples are presented in Figure 2. PVA powder shows peaks at 3408 (O−H stretch), 2941 (CH_2 asymmetric stretch), 1659 (C═O stretch), 1445 (CH_2 bend), 1383 (CH_2 wag), 1329 (in-plane C−H and O−H bend), 1238 (C−H wag), 1146 (C−C and C−O−C stretch), and 1098 cm^{-1} (C−O−C stretch).[33] The peak around 1146 cm^{-1} is related to the crystallinity of PVA.[34] The peak at 1098 cm^{-1} is the characteristic peak of the PVA main chain associated with the C−O−C stretching vibration.[35] The CHLE peaks appear at 3408 (O−H stretch), 2928 (aliphatic C−H stretch), 1616 (C═C stretch), 1514 (C−H bend), 1383 (O−H bend), 1263 (C−N stretch), and 1074 cm^{-1} (C−O stretch).[36] The peak at 2928 cm^{-1} indicates the aliphatic C−H stretching vibration, which is the characteristic peak of CHLE associated with citronellal.[37] The SA peaks were found at 3441 (O−H stretch), 2928 (C−H stretch), 1614 (O−C−O asymmetric stretch), 1414 (O−C−O symmetric stretch), 1306 (C−C−H deformation), and 1030 cm^{-1} (C−O stretch).[38]

The peaks at 1614 and 1414 cm^{-1} prove the presence of the O−C−O asymmetric stretching vibration and O−C−O symmetric stretching vibration, which are the characteristic peaks of SA.[39] The CS peaks appear at 3449 (O−H and N−H stretch), 2922 (C−H stretch), 1614 ($-NH_2$ bend), 1422 (CH_2 bend), 1383 (CH_3 symmetrical deformation), 1327 (C−N stretch), and 1059 cm^{-1} (C−O stretch).[40] The peak around 1614 cm^{-1} proves the presence of bending vibrations of the amine group ($-NH_2$), which is the characteristic peak of CS.[41]

The characteristic peak for PVA powder (1098 cm^{-1}) is represented by peaks at 1015, 1036, 1032, 1049, and 1094 cm^{-1} for PVA, PVA/CHLE, PVA/CHLE/CS, PVA/CHLE/SA, and PVA/CHLE/SA/CS hydrogels, respectively. The characteristic peak of CHLE (2928 cm^{-1}) is observed for all composite hydrogels at nearly identical wavenumbers. The characteristic peak is indicated by the wavenumbers of 2922, 2922, 2922, and 2924 cm^{-1} for PVA/CHLE, PVA/CHLE/CS, PVA/CHLE/SA, and PVA/CHLE/SA/CS hydrogels, respectively. The characteristic peaks for SA (1614 and 1414 cm^{-1}) are observed for the two composite hydrogels, namely, PVA/CHLE/SA hydrogel (1630 and 1439 cm^{-1}) and PVA/CHLE/SA/CS hydrogel (1632 and 1441 cm^{-1}).

Lastly, the characteristic peak for CS (1614 cm^{-1}) is represented by the peaks at 1628 cm^{-1} for the PVA/CHLE/CS hydrogel and 1632 cm^{-1} for the PVA/CHLE/SA/CS hydrogel. Thus, it can be concluded that PVA, CHLE, CS, and SA are successfully loaded in the composite hydrogel. The changes in characteristic peaks are caused by the physical mixture and chemical interactions that occur when two or more polymers are mixed. These changes indicate the good miscibility between polymers.[42]

3.3. XRD Characterization. The XRD profiles of the powder and hydrogel samples are shown in Figures S1 and 3,

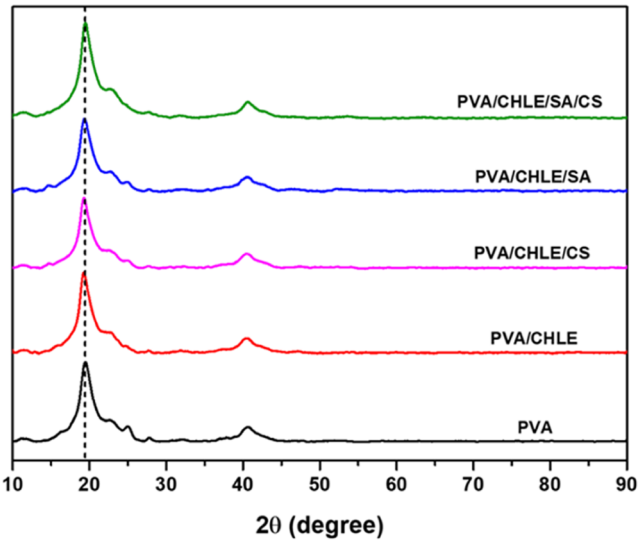

Figure 3. XRD spectra of the hydrogel samples.

respectively. From the diffraction pattern, the PVA powder appears to be semicrystalline, similar to the previous study.[43] There is a sharp peak at 2θ = 19.57°, a shoulder peak at 2θ = 22.53°, and a secondary peak at 2θ = 40.67°. These three peaks correspond to the lattice sizes d = 4.53, 3.94, and 2.22 Å, respectively, and are associated with the reflection planes (101), (200), and (102).[20] The crystallinity degree was obtained from the ratio between the area under the maximum peak and the total area of the spectrum. The crystallinity of the PVA powder was found to be 58.59%, close to the previous study.[20]

CHLE powder exhibits a diffraction peak at 2θ = 18.95°, which refers to the lattice size of 4.64 Å. At 2θ over 35°, the spectrum is broad and sloping, which indicates the amorphous nature of the CHLE powder. CS powder is semicrystalline as

https://doi.org/10.1021/acsomega.3c10143
ACS Omega 2024, 9, 13306−13322

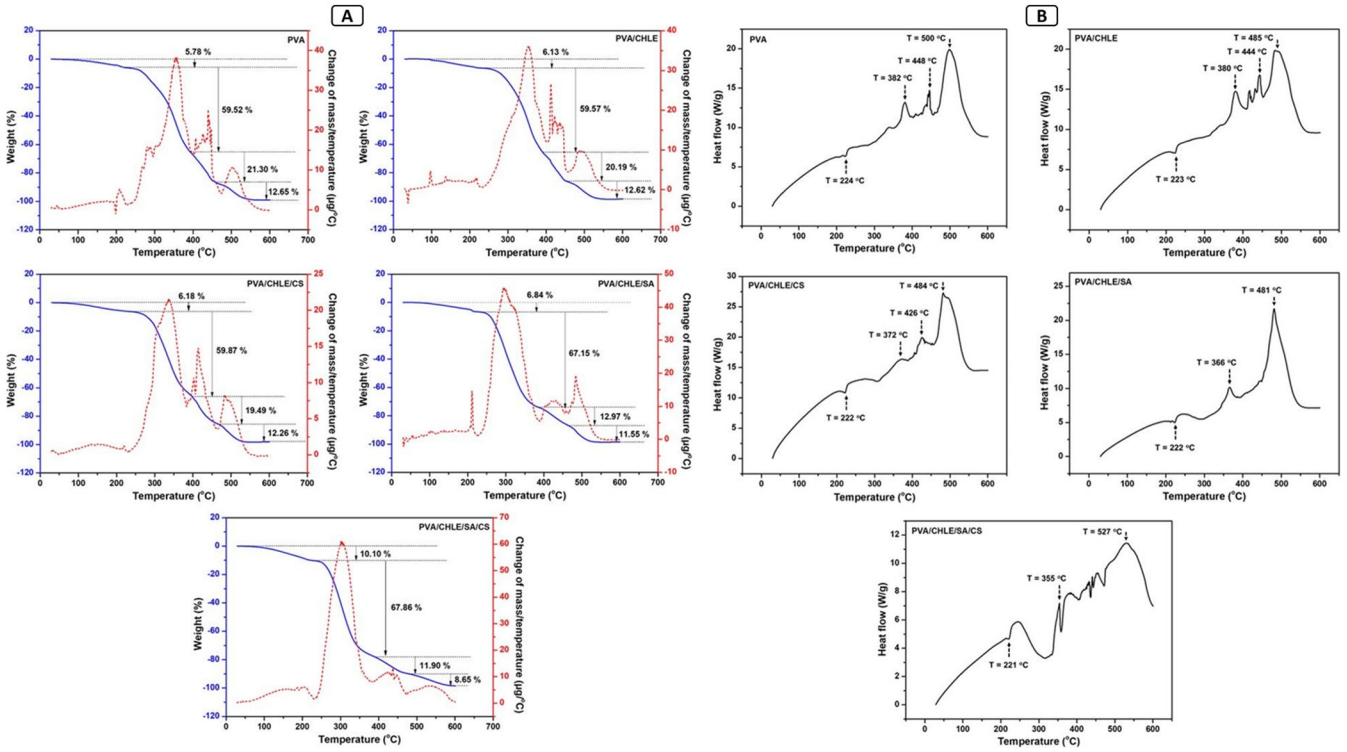

Figure 4. (A) TGA analysis of the hydrogel samples and (B) thermograms of the hydrogel samples.

indicated by its spectrum profile, in accordance with the previous study.[44] The main diffraction peak is located at 2θ = 20.20°, with a lattice size of d = 4.39 Å, which comes from the reflection plane (220).[44] At 2θ from 33 to 70°, the diffraction pattern gradually slopes down, which corresponds to the amorphous region of the CS.[45] The crystallinity the CS powder was found to be 56.67%, close to the previous study.[46] SA powder exhibits semicrystalline properties derived from the interaction between SA chains through hydrogen bonds.[47] Peak diffraction lies at a 2θ of about 13.71, 21.63, and 36.50°, which refers to the lattice sizes d = 6.45, 4.10, and 2.46 Å, respectively, and corresponds to the reflection plane (110) of the poly guluronate unit, (200) of the polymannuronate unit, and halo.[48] The crystallinity of the SA powder was found to be 28.72%, close to the previous study.[49]

In Figure 3, all hydrogels were found to be semicrystalline because the PVA fraction dominated the hydrogel composition. The diffraction peak is located at 2θ around 19.41°. The crystallinity degree of the PVA, PVA/CHLE, PVA/CHLE/CS, PVA/CHLE/SA, and PVA/CHLE/SA/CS hydrogels was approximately 51.94, 49.86, 47.31, 45.87, and 43.04%, respectively. The PVA hydrogel has a lower crystallinity degree than that of PVA powder. The freeze−thaw process causes a change in the orientation of the PVA chain, which was originally aligned in PVA powder and then became unaligned in the PVA hydrogel, so that the crystallinity degree decreases.[20] These results were also confirmed by the decrease in peak intensity at a wavenumber of around 1146 cm^{-1} in the FTIR spectra. The PVA/CHLE hydrogel was found to have a lower crystallinity degree than that of the PVA hydrogel. The lower crystallinity showed that the PVA hydrogel was affected by the amorphous nature of CHLE. The loading of CS to the PVA/CHLE hydrogel caused even lower crystallinity since amine groups of CS can interact with the hydroxyl groups of PVA to form hydrogen bonds, thereby interfering with the formation of PVA crystals.[50] The loading of SA in the PVA/CHLE hydrogel also resulted in a lower crystallinity degree since SA is known to cause a diluting effect, thereby interfering with PVA crystallization.[51] Lastly, the PVA/CHLE hydrogel loaded with SA and CS showed the lowest crystallinity degree compared to other hydrogels due to the combined effect of loading effects of SA and CS, as previously described. In addition, the blend of SA and CS is known to produce polyelectrolyte complexes, where the hydrogen bonds between the amino groups and the hydroxyl groups in CS will be broken when interacting with SA, thereby reducing the crystallinity degree.[52] XRD characterization is important to determine the degree of crystallinity of the hydrogel.

3.4. Thermal Properties. The thermal characterization carried out in this study included TGA and DSC. TGA characterization was carried out to identify the thermal stability of the hydrogel against temperature changes. Meanwhile, DSC characterization was used to analyze the crystallinity degree of hydrogels to complement and confirm XRD data.[20]

3.4.1. Thermogravimetric Analysis (TGA). The TGA analysis of the powder samples and the hydrogel samples is presented in Figures S2 and 4. (a) The thermogravimetric analysis includes the onset temperature, maximum temperature of differential thermal gravimetry (DTG), and residue at 600 °C, as shown in Table 1. The onset temperature was obtained from the intersection of the baseline mass and tangent drawn to the mass curve at the point where the sample underwent significant mass decomposition.[53] PVA powder experienced three decomposition phases at less than 122 °C (evaporation of water molecules), 196−375 °C (decomposition of the hydroxyl groups/side groups), and 397−526 °C (decomposition of the carbonyl groups/backbones).[20,54,55] After heating to 600 °C, the PVA powder left a residue of about 1.60%, which is the inorganic part of PVA.[56]

https://doi.org/10.1021/acsomega.3c10143
ACS Omega 2024, 9, 13306−13322

Table 1. Thermal Properties of the Samples Extracted from the TGA Analysis

sample name	onset temperature (°C)	temperature at the maximum of DTG (°C)	residue at 600 °C (%)
PVA powder	257	341, 483	1.60
CHLE powder	239	123, 281, 404	26.87
CS powder	271	295	33.95
SA powder	230	244	35.74
PVA hydrogel	300	356, 440, 504	0.96
PVA/CHLE hydrogel	294	353, 436, 494	1.43
PVA/CHLE/CS hydrogel	286	336, 430, 485	1.93
PVA/CHLE/SA hydrogel	263	317, 427, 483	1.44
PVA/CHLE/SA/CS hydrogel	262	304, 422, 524	1.53

For CHLE powder, decomposition occurred at a temperature of less than 170 °C, related to the chemical compounds in CHLE (neryl acetate and α-humulene),[3] which are known to decompose at 134 and 166 °C, respectively.[57,58] Significant decomposition then occurred at 175−305 °C, related to the decomposition of citronellal, linalool, γ-terpinène, and nerolidol,[3] which are known to decompose at 207, 198, 183, and 276 °C, respectively.[59,60] At 370−566 °C, the complete decomposition of the extract then took place, leaving a residue of about 26.87%. CS powder experienced three decomposition phases at less than 105 °C (evaporation of water molecules), 246−300 °C (dehydration of the saccharide ring),[61] and 300−572 °C (complete decomposition of CS), leaving a residue of about 33.95% in the form of carbon.[62] There were three decomposition phases of SA powder at less than 102 °C (evaporation of water molecules), 212−263 °C (breakdown of glycosidic bonds), and 273−564 °C (formation of Na_2CO_3).[63] At the end of heating, there was a residue of about 35.74%, associated with the carbonized material.[64]

The PVA hydrogel showed a higher onset temperature and maximum temperature of DTG than those of PVA powder, indicating higher thermal stability. This is related to the formation of hydrogen bonds between PVA hydroxyl groups during freeze−thaw.[20] At the end of heating, the residue left was about 0.96%, lower than that of PVA powder. The loading of extract in the PVA hydrogel then resulted in a lower onset temperature and maximum temperature of DTG. During the heating, the extract accumulates heat, thereby reducing the thermal stability of the hydrogel.[20] The resulting residue increased to 1.43% because the residue of extract powder was greater than that of PVA powder.

The loading of CS then caused a decrease in the onset temperature and maximum temperature of DTG of the PVA/CHLE hydrogel. This relates to the loading effect of CS, where CS is known to interfere with hydrogen bond formation in the PVA hydrogel, which causes its thermal stability to decrease.[65] The resulting residue increased to about 1.93% due to the addition of residue from CS. The decreased thermal stability was also observed after loading of SA in the PVA/CHLE hydrogel. This can be seen in the decrease of onset temperature and maximum temperature of DTG, where SA is known to weaken the hydrogen bonds in the PVA hydrogel, thereby reducing its thermal stability.[66] Due to the addition of residue from SA, the residue left increased to 1.44%.

Moreover, the loading of SA and CS simultaneously resulted in a decrease in the onset temperature and maximum temperature of DTG of the PVA/CHLE hydrogel. The decrease in thermal stability was related to the restructuring of the cross-links in the PVA/CHLE hydrogel after loading of SA and CS, as previously described. However, a higher maximum temperature of DTG was observed in the last decomposition phase, which may be related to the decomposition of carbonaceous materials from SA and CS to leave a residue. The resulting residue increased to 1.53% due to the addition of SA and CS residues.

3.4.2. Differential Scanning Calorimetry (DSC). The thermograms of the powder samples and hydrogel samples are presented in Figures S3 and 4b. The analysis on the thermal properties includes the peak temperature of exothermic and endothermic processes and the crystallinity degree, as shown in Table 2. For powder samples, the peak temperature of exothermic and endothermic processes described the decomposition phases, according to the TGA profile. An endothermic peak was found at 222 °C for the PVA powder, which is the melting point of PVA powder, similar to the previous study.[20] The enthalpy change was calculated from the area around the endothermic peak (196−230 °C), which was found to be around 81.34 J/g. The enthalpy change at the melting point of PVA with a crystallinity degree of 100% is known to be 138.60 J/g.[64] The crystallinity degree of PVA powder was then calculated from the ratio between the enthalpy change of the sample (ΔH) and 138.60 J/g (ΔH_0), as shown in eq 2

Table 2. Thermal Properties of the Samples Extracted from the Thermograms

sample name	peak temperature in the exothermic process (°C)	peak temperature in the endothermic process (°C)	enthalpy change at the melting point of PVA, ΔH (J/g)	degree of crystallinity (%)
PVA powder	319, 383, 480	222	81.34	58.69
CHLE powder		125, 245, 550		
CS powder	294, 370	59		
SA powder	249, 352	50		
PVA hydrogel	382, 448, 500	224	71.71	51.74
PVA/CHLE hydrogel	380, 444, 485	223	68.76	49.61
PVA/CHLE/CS hydrogel	372, 426, 484	222	65.78	47.46
PVA/CHLE/SA hydrogel	366, 481	222	62.85	45.35
PVA/CHLE/SA/CS hydrogel	355, 527	221	59.60	43.00

https://doi.org/10.1021/acsomega.3c10143
ACS Omega 2024, 9, 13306−13322

Table 3. Texture Profile Analysis (TPA) Results for the Hydrogels

hydrogel sample	hardness (gForce)	adhesiveness (g s)	springiness (%)	cohesiveness (%)	gumminess (gForce)	chewiness (gForce)	resilience (%)
PVA	2878.8797	−20.0190	0.8140	0.9633	2771.9463	2269.7197	1.2000
PVA/CHLE	3550.8053	−19.7770	0.8510	0.9343	3318.7910	2860.0200	1.1690
PVA/CHLE/CS	3508.0047	−31.1440	0.8660	0.9280	3253.9810	2848.3307	1.1040
PVA/CHLE/SA	3272.4580	−9.7090	0.8037	0.9173	3000.9353	2433.6960	1.0803
PVA/CHLE/SA/CS	3354.1883	−11.8920	0.9047	0.9130	3061.1000	2767.6857	1.0920

$$X = \frac{\Delta H}{\Delta H_0} \times 100\% \quad (3)$$

The crystallinity degree of the PVA powder was about 58.69%, close to the XRD results. The crystallinity degree is associated with the PVA fraction in the hydrogel and confirmed the crystallinity degree obtained from XRD results.[20]

For hydrogel samples, the PVA hydrogel showed a lower crystallinity degree than that of the PVA powder. The decrease was due to the reduced number of the PVA chains folding and the lamellar thickness of PVA crystals during the freeze−thaw process.[20] The melting point and crystallinity of the PVA/CHLE hydrogel were found to be lower than those of the PVA hydrogel. The loading of CHLE caused the PVA fraction in the PVA/CHLE hydrogel to decrease. Hence, the melting point shifted toward a lower temperature, and the amount of heat to melt the PVA in the hydrogel reduced.[20] The loading of CS in the PVA/CHLE hydrogel reduced the melting point and the crystallinity even further, which matched that of the previous study. In the earlier study, the crystallinity degree of the PVA hydrogel decreased after the loading of CS.[67] It was explained that the free PVA molecules accumulated to form crystals during freeze−thaw, whereas the PVA molecules interacting with CS molecules did not join the crystal formation and were left out.[67]

In addition, the loading of CS also reduced the PVA fraction in the hydrogel, thereby lowering its crystallinity. The decrease in the melting point and crystallinity degree of the PVA/CHLE hydrogel was also observed after the loading of SA. The loading of SA meant that the PVA fraction in the hydrogel was reduced, so the crystallinity was also decreased. This result is in line with the previous research,[51] where the melting point of the PVA hydrogel shifted to a lower temperature after the loading of SA. The reduced endothermic peak area also indicated a reduction in the crystallinity of the PVA hydrogel. The reduction was due to the reduced hydrogen bonding between PVA chains after loading of SA.[51]

Lastly, the loading of SA and CS in the PVA/CHLE hydrogel resulted in the lowest melting point and crystallinity degree among other hydrogel samples, since the PVA fraction in the PVA/CHLE/SA/CS hydrogel was the lowest compared to the other hydrogels. In addition, SA and CS also had an effect on reducing the crystallinity of the hydrogel, as previously described. From Table 2, it was found that the crystallinity of the hydrogel obtained from DSC confirmed the crystallinity degree obtained from XRD. In addition, the peak temperature in the exothermic and endothermic processes shifted to a lower temperature, which indicated a decrease in the thermal stability of the hydrogel, as described in its TGA profile.

3.5. Gel Fraction. Following immersion in PBS for 48 h, a noticeable change occurred as the initially clear solution turned yellowish due to the extract released from the hydrogel during testing. The comparison between the mass of the redried hydrogel post-test and the mass of the initially dried hydrogel, referred to as gel fraction,[20] provided insights into solubility. The PVA hydrogel exhibited the highest gel fraction at 98.15 ± 0.34^{d}%, indicating almost complete cross-linking of PVA chains.[68] However, upon loading CHLE, the gel fraction decreased to 96.08 ± 0.11^{c}%, attributed to CHLE release, causing a higher weight loss than the PVA hydrogel. Further reduction in the gel fraction was observed in the PVA/CHLE hydrogel after CS addition (94.59 ± 0.33^{ab}%) and in the PVA/CHLE/SA hydrogel (95.19 ± 0.21^{b}%), as SA and CS are known to have low cross-linking behavior.[18,69]

The lowest gel fraction was noted in the PVA/CHLE/SA/CS hydrogel at 94.24 ± 0.14^{a}%, attributed to SA and CS loading effects and increased hydrogel brittleness from elevated weight loss.[24] Significant differences ($p < 0.05$) in the gel fraction were observed between PVA/CHLE and PVA/CHLE/CS, PVA/CHLE/SA, and PVA/CHLE/SA/CS hydrogels. The gel fraction of all samples, surpassing 90%, indicates the extent of cross-linking in the hydrogel matrix. A higher gel fraction signifies enhanced robustness, durability, and reduced solubility in water, offering a distinct advantage to the characteristics of these hydrogels.[70] Given the relationship between the gel fraction, cross-linking content, and weight loss, these hydrogel combinations hold promise for potential applications as wound dressings with a high cross-linking content.

3.6. Texture Profile Analysis (TPA). The results of the TPA test are listed in Table 3. Hardness is the maximum peak at the first pressure of the hydrogel.[71] In Table 3, it can be seen that the CHLE loading in the PVA hydrogel resulted in an increase in hardness. The PVA/CHLE hydrogel that received CS loading then showed a decrease in hardness. Lower levels of hardness were also observed after SA loading in the PVA/CHLE hydrogel. The loading of SA/CS in the PVA/CHLE hydrogel then resulted in hardness between the PVA/CHLE/CS hydrogel and PVA/CHLE/SA hydrogel. Adhesiveness is the adhesive power of the hydrogel.[71] For hydrogel adhesiveness, CHLE loading in the PVA hydrogel resulted in an increase in adhesiveness. The CS-loaded PVA/CHLE hydrogel then showed a decrease in the adhesiveness. Enhancement in the adhesiveness of the PVA/CHLE hydrogel was then observed after SA loading.

The loading of SA/CS in the PVA/CHLE hydrogel then resulted in adhesiveness between the PVA/CHLE/CS hydrogel and PVA/CHLE/SA hydrogel. Springiness or elasticity can be interpreted as the recovery time between the end of the first pressure and the beginning of the second pressure.[71] The loading of CHLE in the PVA hydrogel resulted in an increase in springiness. The PVA/CHLE hydrogels that received CS loading then showed an improvement in springiness. Declined springiness of the PVA/CHLE hydrogel was then observed after SA loading. The loading of SA/CS in the PVA/CHLE hydrogel then yielded the highest springiness. Cohesiveness is

https://doi.org/10.1021/acsomega.3c10143
ACS Omega 2024, 9, 13306−13322

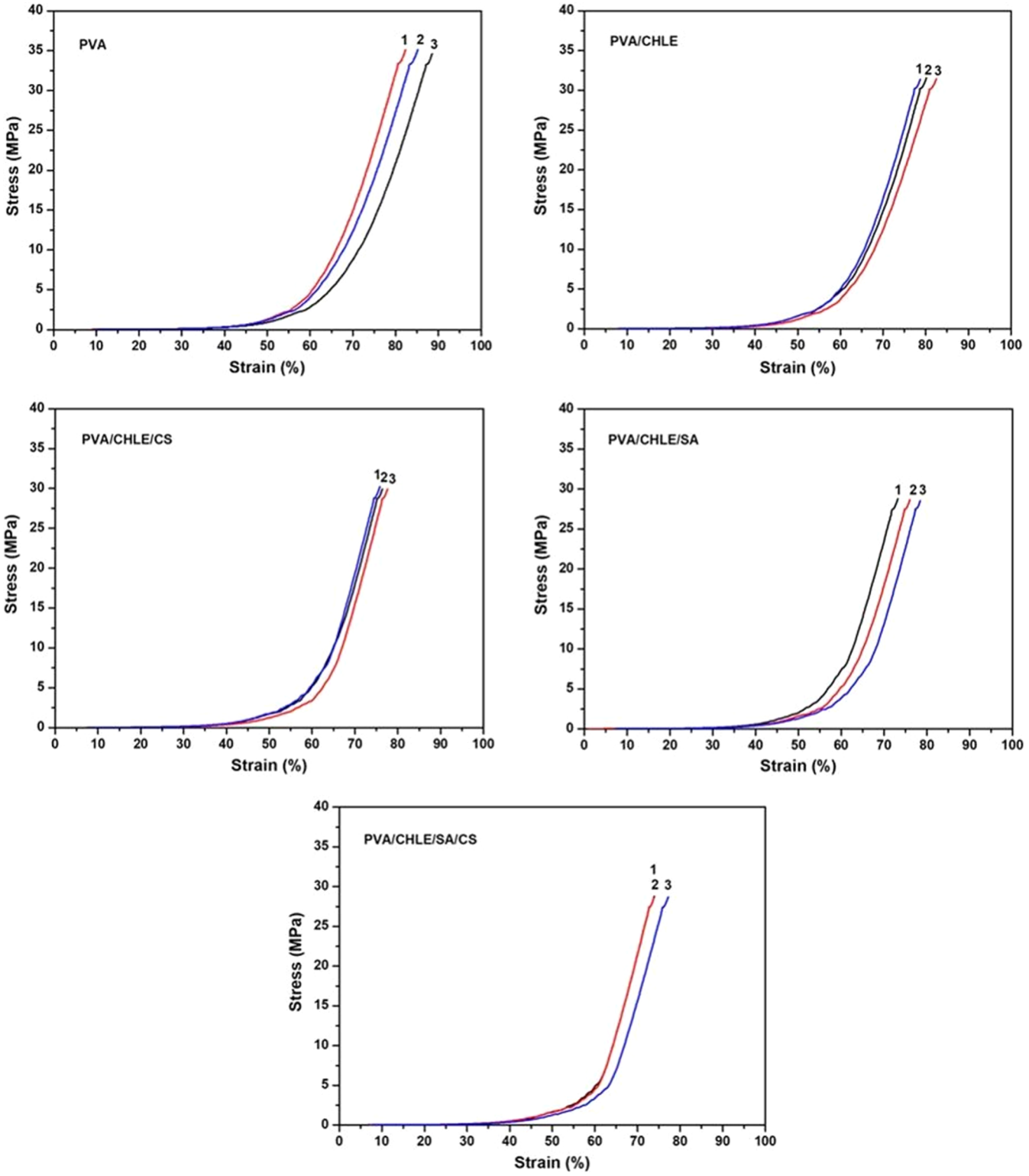

Figure 5. Stress−strain graphs of the hydrogels.

defined as the ratio of the pressure area during the second compression to that during the first compression. Cohesiveness can be measured as the degree to which materials are destroyed mechanically.[71]

For hydrogel cohesiveness, CHLE loading in the PVA hydrogel resulted in a decrease in cohesiveness. The PVA/CHLE hydrogel that received CS loading then showed decreased cohesiveness. Lower cohesiveness was also observed after SA loading in the PVA/CHLE hydrogel. SA/CS loading in the PVA/CHLE hydrogel then produces the lowest cohesiveness value. Gumminess is defined as the result of calculating the value of hardness times the value of cohesiveness.[71] Loading CHLE in the PVA hydrogel resulted in an increase in gumminess. The CS-loaded PVA/CHLE hydrogel then showed decreased gumminess. Declined gumminess of PVA/CHLE hydrogels was then also observed

https://doi.org/10.1021/acsomega.3c10143
ACS Omega 2024, 9, 13306−13322

Table 4. Compressive Strength of the Hydrogels[a]

	compressive strength			
hydrogel sample name	maximum stress (MPa)	onset strain (%)	onset stress (MPa)	compressive modulus (MPa)
PVA	34.9468 ± 0.3111^{e}	65.7995 ± 3.0760^{b}	0.0536 ± 0.0018^{c}	187.0515 ± 0.4792^{d}
PVA/CHLE	31.4583 ± 0.0819^{d}	62.7062 ± 1.8850^{ab}	0.0474 ± 0.0001^{b}	183.8655 ± 0.4780^{c}
PVA/CHLE/CS	30.0180 ± 0.1706^{c}	61.0730 ± 1.4927^{ab}	0.0466 ± 0.0006^{ab}	179.0026 ± 0.2252^{b}
PVA/CHLE/SA	29.1802 ± 0.1130^{b}	60.5062 ± 1.6099^{ab}	0.0453 ± 0.0013^{ab}	178.1596 ± 0.7240^{b}
PVA/CHLE/SA/CS	28.6879 ± 0.0791^{a}	60.1048 ± 1.4850^{a}	0.0431 ± 0.0004^{a}	176.4502 ± 0.2491^{a}

[a]The values were expressed as the mean ± standard deviation of the three samples (n = 3). The use of superscripts in each column indicates a statistically significant difference between groups. In each column, values with different superscripts showed significant differences (p < 0.05).

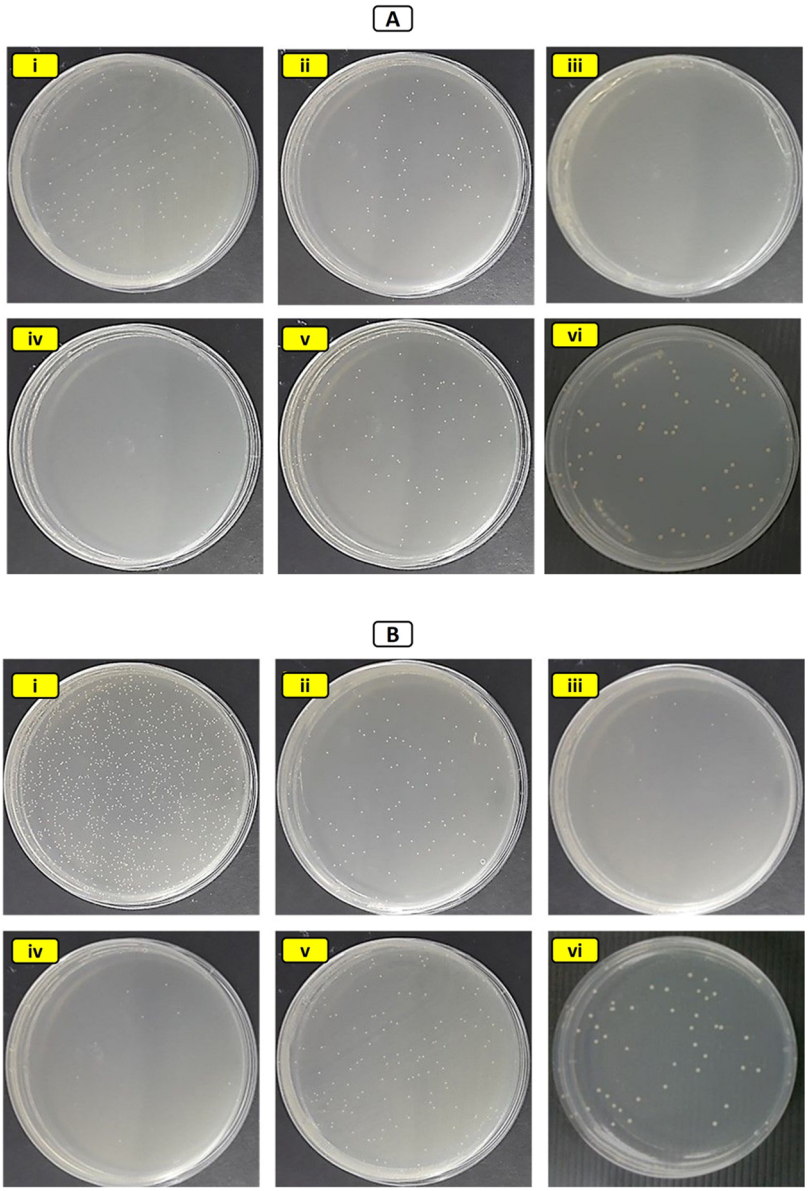

Figure 6. (A) Colonies of *S. aureus* from (i) control and (ii) PVA, (iii) PVA/CHLE, (iv) PVA/CHLE/CS, (v) PVA/CHLE/SA, and (vi) PVA/CHLE/SA/CS hydrogels. (B) Colonies of *P. aeruginosa* from (i) control and (ii) PVA, (iii) PVA/CHLE, (iv) PVA/CHLE/CS, (v) PVA/CHLE/SA, and (vi) PVA/CHLE/SA/CS hydrogels.

after SA loading. The loading of SA/CS in the PVA/CHLE hydrogel then resulted in gumminess between the PVA/CHLE/CS hydrogel and PVA/CHLE/SA hydrogel.

Chewiness is defined as the result of calculating the value of gumminess multiplied by the value of springiness.[71] Loading of CHLE in the PVA hydrogel resulted in an increase in chewiness. The PVA/CHLE hydrogel that received CS loading then showed a decrease in the chewiness. Declined chewiness of the PVA/CHLE hydrogel was then observed after SA loading. The loading of SA/CS in the PVA/CHLE hydrogel then resulted in chewiness between the PVA/CHLE/CS hydrogel and PVA/CHLE/SA hydrogel. Resilience is the

https://doi.org/10.1021/acsomega.3c10143
ACS Omega 2024, 9, 13306−13322

Table 5. Antibacterial Activity of the Hydrogels

sample name	log of the number of *S. aureus* colonies after 24 h of incubation (cfu/mL)	antibacterial activity (% per gram) against *S. aureus*	log of the number of *P. aeruginosa* colonies after 24 h of incubation (cfu/mL)	antibacterial activity (% per gram) against *P. aeruginosa*
control	8.10 ± 0.04^{d}		9.17 ± 0.24^{c}	
PVA	7.99 ± 0.06^{d}	1.16 ± 0.77^{a}	8.71 ± 0.03^{bc}	3.76 ± 0.74^{ab}
PVA/CHLE	2.33 ± 0.26^{b}	59.75 ± 1.17^{b}	8.32 ± 0.01^{b}	7.66 ± 0.45^{c}
PVA/CHLE/CS	1.15 ± 0.21^{a}	62.02 ± 5.37^{b}	4.23 ± 0.16^{a}	29.75 ± 1.43^{d}
PVA/CHLE/SA	7.67 ± 0.09^{d}	4.05 ± 1.47^{a}	8.86 ± 0.02^{bc}	2.64 ± 0.18^{a}
PVA/CHLE/SA/CS	4.03 ± 0.34^{c}	44.50 ± 8.03^{b}	8.47 ± 0.10^{b}	6.78 ± 0.94^{bc}

measurement of the degree of recovery of sample deformation seen in terms of speed and strength.[71] For hydrogel resilience, CHLE loading in the PVA hydrogel resulted in a decrease in resilience. The PVA/CHLE hydrogel that received CS loading then showed a decreased resilience. Resilience levels were also observed after SA loading in the PVA/CHLE hydrogel. The loading of SA/CS in the PVA/CHLE hydrogel then resulted in resilience between the PVA/CHLE/CS hydrogel and PVA/CHLE/SA hydrogel. Hydrogels for topical applications must have high adhesion, high cohesiveness, and low hardness.[72]

3.7. Compression Test. The stress−strain graphs obtained from the compressive strength test of the hydrogels are shown in Figure 5. The compressive strength, onset strain, onset stress, and compressive modulus extracted from the stress−strain graphs are presented in Table 4. The compressive strength represents the maximum stress that the hydrogel can accept. Onset strain and onset stress are the point of intersection between two tangential lines connected from the low-stress and high-stress regions. The compressive modulus is obtained from the slope of the stress−strain graphs in the high-stress region.[21]

For each hydrogel, the test was carried out three times, and then, the average value was presented. The stress−strain graphs obtained show a typical shape resembling the letter "J".[21] The shape results from the interaction between the compressive force and the hydrogel changes during the test. Initially, the hydrogel containing the liquid is soft. When a compressive force is applied, the hydrogel will release the liquid because the shape of the hydrogel changes to a flat shape with the polymer chains tending to be in the same direction. The hydrogel then becomes harder, so that with a continuously applied compressive force, a graphic shape resembling the letter "J" will be produced.[20,21]

The compressive strength of the PVA hydrogel showed the highest value among other hydrogel samples, resulting in a hydrogel with rigid properties. The rigid nature comes from the PVA hydroxyl groups, which are cross-linked. The cross-linking causes the crystallinity of the PVA hydrogel to be high, resulting in high compressive strength.[73] The compressive strength of the PVA hydrogel then decreased after loading CHLE. This is related to the CHLE, which contains the ethanol fraction, which does not freeze during freeze−thaw. The ethanol acts as a free liquid in the PVA/CHLE hydrogel, causing the hydrogel to become softer.[20] The loading of CS in the PVA/CHLE hydrogel then resulted in a lower compressive strength. This result is related to the loading effect of CS, where loading of CS in the PVA hydrogel is known to result in lower cross-linking density.[74]

In addition, CS is also known to play a role in disrupting the formation of crystal networks from the PVA hydrogel, thereby reducing its compressive strength,[75] as confirmed by the decrease of the crystallinity degree in the XRD and DSC data. The decrease in the compressive strength of the PVA/CHLE hydrogel was also observed after loading of SA. This is related to the loading effect of SA, where loading of SA in the PVA hydrogel is known to weaken the hydrogen bonds, thereby reducing the cross-linking density and crystallinity,[66] as confirmed by the XRD and DSC data. Therefore, the resulting compressive strength also decreases.

Furthermore, loading of SA and CS in the PVA/CHLE hydrogel resulted in the lowest compressive strength among other hydrogel samples. The result was due to the loading effect of SA and CS, as previously described. In addition, mixing of SA and CS solutions is known to cause inhomogeneous precipitation, in which a polyion complex is formed at the interface of the two solutions, thereby stopping further reactions. As a result, the density of cross-linking formed in the hydrogel becomes lower, thereby lowering its compressive strength.[76] The results of the compressive strength test are corroborated by data on the crystallinity degree from XRD and DSC, where the lower crystallinity degree is associated with the lower compressive strength.

Statistical tests on maximum stress showed that there was a significant difference between groups ($p < 0.05$). Wang et al.[77] have reported a very strong and resilient hydrogel with a compressive modulus of around 217 MPa, higher than the skin's compressive modulus of around 100 MPa. The hydrogel has versatile functionality, especially as a structural element. With a compressive modulus ranging from 176 to 187 MPa, the hydrogel produced in this study has very strong mechanical properties, so it has the potential to be applied as a wound dressing, which is strong against pressure from both body movements and external objects.

3.8. In Vitro Antibacterial Activity. The results obtained for the inhibition zone against *S. aureus* and *P. aeruginosa* are presented in Figures S4 and S5. The number of colonies of *S. aureus* and *P. aeruginosa* for each hydrogel sample is presented in Figure 6A,B. The results of the analysis are presented in Table 5. In simple terms, the better antibacterial activity is indicated by the formation of fewer bacterial colonies.[78] The PVA hydrogel showed the lowest antibacterial activity among other hydrogel samples, namely, 1.16 ± 0.77^{a} and 3.76 ± 0.74^{ab}% per gram. These results are related to the nature of the PVA hydrogel, where PVA is known to have no antibacterial activity.[79] The presence of this small antibacterial activity was thought to be caused by the release of water from the hydrogel, which pushed the bacteria away from the edge of the hydrogel, thereby disrupting the growth of these bacteria.[20]

The loading of CHLE in the PVA hydrogel then resulted in higher antibacterial activity, namely, 59.75 ± 1.17^{b} and 7.66 ± 0.45^{c}% per gram. These results proved that the CHLE has the antibacterial activity derived from citronellal compounds as the main ingredient.[3,4] The presence of citronellal was confirmed at a wavenumber of about 2928 cm^{-1} in the FTIR spectra.

https://doi.org/10.1021/acsomega.3c10143
ACS Omega 2024, 9, 13306−13322

Citronellal interacts strongly with molecules on the bacterial cell surface such as membrane proteins and other molecules for bacterial growth. After binding to the molecules, citronellal forms a single layer, which alters the electrostatic potential and hydrophobicity of the bacterial cell. This causes damage to the bacterial cell membrane and results in the release of internal cellular molecules from the bacterial cell.[80] The PVA/CHLE/CS hydrogel showed the highest antibacterial activity, which was at 62.02 ± 5.37^{b} and 29.75 ± 1.43^{d}% per gram. These results relate to the loading effect of CS, where CS is known to have high intrinsic antibacterial activity, as confirmed in a previous study.[24]

In addition, chitosan also has an amine functional group (NH_2), which is positively charged, so that it can form bonds with a negatively charged bacterial cell wall, as confirmed in the FTIR spectrum at 1614 cm^{-1}. The formed bonds cause cell disruption, change in cell membrane permeability, inhibition of DNA replication, and bacterial cell death.[81] The loading of SA in the PVA/CHLE hydrogel then was observed to produce a decrease in antibacterial activity, which was at 4.05 ± 1.47^{a} and 2.64 ± 0.18^{a}% per gram, since SA does not have any intrinsic antibacterial ability.[82] In addition, it was possible that the loading of SA restrained the release of the extract during the test, thereby decreasing its antibacterial activity, as confirmed by the release test in the next section.

Furthermore, the PVA/CHLE hydrogel loaded with SA and CS showed an antibacterial activity of around 44.50 ± 8.03^{b} and 6.78 ± 0.94^{bc}% per gram, respectively, higher than that of the PVA/CHLE/SA hydrogel but lower than that of the PVA/CHLE hydrogel. These results were related to the loading effects of SA and CS, as previously described. Antibacterial activity against *S. aureus* did not show significant differences between groups for PVA/CHLE, PVA/CHLE/CS, and PVA/CHLE/SA/CS hydrogels ($p > 0.05$). However, between PVA and PVA/CHLE hydrogels as well as between PVA/CHLE and PVA/CHLE/SA hydrogels, there was a significant difference ($p < 0.05$). On the other hand, antibacterial activity against *P. aeruginosa* showed that the PVA/CHLE hydrogel had a significant difference with the PVA, PVA/CHLE/CS, and PVA/CHLE/SA hydrogels ($p < 0.05$) but did not have a significant difference with the PVA/CHLE/SA/CS hydrogel ($p > 0.05$). In general, the antibacterial activity of the hydrogel samples against *S. aureus* was higher than that against *P. aeruginosa*, except for the PVA hydrogel. This is due to the composition of the cell wall of each bacterium, where *S. aureus* has a peptidoglycan layer and *P. aeruginosa* has peptidoglycan, lipopolysaccharide, and phospholipids, which act as a barrier to antibacterial substances.[83]

3.9. Release Test. The release profile of the extract for hydrogels is presented in Figure 7. All hydrogel samples initially experienced burst release within 20 min, which was expected to be the release of extract from the hydrogel surface through a rapid diffusion mechanism.[23] Moreover, the extract buried in the hydrogel was also be released. This is similar to the previous research that the burst phenomenon that happened in many cases was partly due to the formation of pores and cracks in polymeric matrices of the hydrogel.[84] Afterward, the release of extract becomes a more controlled release, also called a sustained release, observed through both the ascending and descending curves along the process. The ascending curve indicates that the concentration of the released extract has increased, while the descending curve indicates the decrease in the concentration of the released extract.[85]

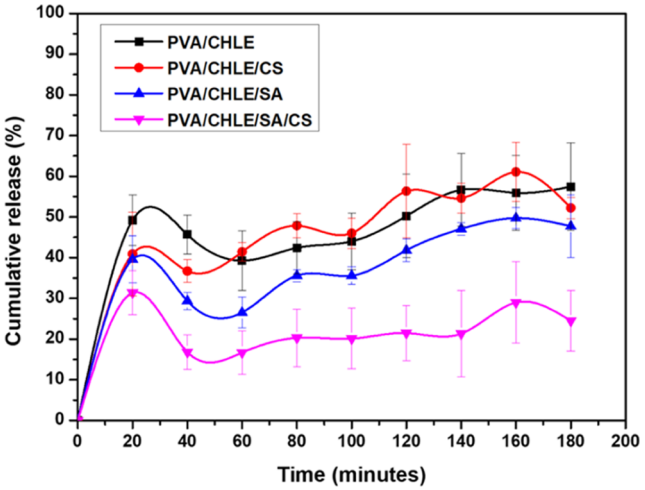

Figure 7. Percentage of cumulative extract release from the hydrogels.

The loading of CHLE in the PVA hydrogel showed the highest cumulative extract release among other hydrogel samples. This indicated that the extract was not fully loaded in the PVA hydrogel so it was easy to erode when interacting with the release medium.[20] The PVA/CHLE/CS hydrogel resulted in lower extract release within the first 60 min, which is related to the loading effect of CS. The interaction between CS and PVA is known to form a strong matrix that prevents the extract release,[86] as confirmed by the hydrogel morphology in the SEM result. After the first 60 min, the extract release was observed to increase at 80, 120, and 160 min, which was related to the sensitivity of CS to the release medium, thus facilitating the release of the extract.[85] The lower extract release was also observed for the PVA/CHLE/SA hydrogel. SA is known to form a barrier to the diffusion transport mechanism, thereby inhibiting the release of the extract.[87] Also, it is possible that the negatively charged group of SA (COO^-) forms cross-linking with the positively charged group of the extract. The extract is known to contain phenolic compounds that can act as a donor of H^+.[88,89] The cross-linking can reduce the release rate of the extract, similar to the previous research.[75] The ability of SA to inhibit the release of the extract also confirmed the decreased antibacterial test result of the PVA/CHLE hydrogel after loading of SA. Lastly, the loading of SA and CS in the PVA/CHLE hydrogel resulted in the lowest extract release among other hydrogel samples. This relates to the loading effects of SA and CS, as previously described. Moreover, SA and CS are also known to form cross-linking through the formation of a polyelectrolyte complex. The polyelectrolyte complex causes hydrogel expansion, resulting in high water absorption, and inhibits the release of the extract.[90]

The data of cumulative extract release from hydrogels are then analyzed based on four models of release kinetics, as shown in eqs 3−6

$$\frac{M_t}{M_\infty} = k_0 t \tag{4}$$

$$\ln\left(1-\frac{M_t}{M_\infty}\right) = -k_1 t \tag{5}$$

https://doi.org/10.1021/acsomega.3c10143
ACS Omega 2024, 9, 13306−13322

Table 6. Modeling of Cumulative Extract Release Data[a]

	zero-order	first-order	Higuchi	Ritger−Peppas		
hydrogel sample name	R^2	R^2	R^2	R^2	k	n
PVA/CHLE	0.7021	0.7885	0.8965	0.9770	16.0377 ± 3.6716^{c}	0.2431 ± 0.0698^{a}
PVA/CHLE/CS	0.7162	0.7777	0.9204	0.9819	13.7007 ± 4.6671^{bc}	0.2856 ± 0.0834^{a}
PVA/CHLE/SA	0.8528	0.9066	0.9681	0.9852	5.3506 ± 2.4054^{ab}	0.4432 ± 0.0986^{a}
PVA/CHLE/SA/CS	0.7564	0.7782	0.9180	0.9702	4.8112 ± 1.9650^{a}	0.3233 ± 0.0990^{a}

[a]The values were expressed as the mean ± standard deviation of the three samples (n = 3). The use of superscripts in each column indicates a statistically significant difference between groups. In each column, values with different superscripts showed significant differences (p < 0.05).

$$\frac{M_t}{M_\infty} = k_h t^{1/2} \quad (6)$$

$$\frac{M_t}{M_\infty} = kt^n \quad (7)$$

where M_t/M_∞ represents the cumulative extract release at time t, t represents the release time, n represents the release exponent, and k_0, k_1, k_h, and k represent the constant for each release kinetics model. Equation 3 represents zero-order kinetics, where the extract release mechanism is controlled by polymer chain relaxation with a constant release rate and does not depend on the concentration.[91] First-order kinetics is represented by eq 4, in which the mechanism of extract release depends on its concentration.[91] The Higuchi model that describes the release of the extract through the Fickian diffusion mechanism is shown by eq 5.[92] Equation 6 shows the Ritger−Peppas model, in which the extract release mechanism depends on the values of n, that are at n < 0.5 (pseudo-Fickian diffusion), n = 0.5 (Fickian diffusion), 0.5 < n < 1 (anomalous transport), and n = 1 (polymer chain relaxation).[93]

Initially, the release of the extract from the hydrogel surface occurred within 20 min of the test, so this initial condition was not taken into account in the release kinetic analysis.[20] The analysis results then show the correlation coefficient (R^2) based on each release kinetics model, as presented in Table 6. In this study, the value of R^2 for hydrogels indicated the Ritger−Peppas model as the most appropriate release kinetics model. The value of n was obtained in the range of 0.2431 ± 0.0698^{a} to 0.4432 ± 0.0986^{a}, which indicates that the mechanism of extract release occurs through pseudo-Fickian diffusion. Pseudo-Fickian diffusion is similar to Fickian diffusion, but the extract release process takes place more slowly.[93] When the extract release occurs through a pseudo-Fickian diffusion, the empty spaces between the polymer chains will be filled by the PBS liquid. The filling process will continue until the volume fraction of the empty space decreases as the volume fraction of the PBS liquid increases.[20]

The statistical test on the value of n did not show a significant difference between groups (p > 0.05). In addition, the value of the kinetic constant (k) indicates the release rate of the extract from the hydrogel. The lower value of k indicates the slower release rate of the extract.[92] The PVA/CHLE/SA/CS hydrogel showed the lowest value of k, so it had the slowest release rate of extract among other hydrogel samples. The hydrogel with slow extract release ability is very good for wound dressing application because it is effective in reducing pain for prolonged application.[94]

3.10. Cytotoxic Activity. Cytotoxic activity of each sample concentration was tested by using normal cells (CV-1). The test was carried out using the Presto Blue method. This method is a good indicator of the 50% inhibitory concentration (IC_{50}) for each sample concentration in various cells.[95] The Presto Blue reagent will then undergo a reduction from the resazurin compound to the resorufin compound when it enters the cell.[96] The resazurin compound is a nonfluorescent blue dye, while the resorufin compound is a fluorescent pink dye.[97] In this test, absorbance measurements are carried out at two wavelengths, namely, 570 nm (resazurin) and 600 nm (resorufin), to produce an absorbance value that shows the number of viable cells after the test. The IC_{50} value is obtained, which shows the concentration threshold for each sample that can be used so that CV-1 cells are still alive at 50%.[98] IC_{50} values for hydrogel samples and cisplatin are shown in Table 7.

Table 7. IC_{50} Values for Hydrogel Samples and Cisplatin

samples	IC_{50} (μg/mL)
PVA	>1000
PVA/CHLE	>1000
PVA/CHLE/CS	>1000
PVA/CHLE/SA	>1000
PVA/CHLE/SA/CS	>1000
cisplatin	13.27

The test results show that all hydrogel samples show IC_{50} values >1000 μg/mL. These results show that all hydrogel samples can be used safely on normal cells up to concentrations above 1000 μg/mL. The test results, IC_{50} calculation graph, and cell morphology at each sample concentration are presented in Figures S6−S11. Based on morphological observations, no cell death occurred at all concentration levels. Other research previously conducted experiments on normal cells of human skin, to examine the safety of *C. hystrix* peel essential oil for topical application on the skin.[99] The results of this research show that *C. hystrix* peel essential oil as well as its main components (limonene, β-pinene, and terpinen-4-ol) is not cytotoxic to normal cells of human skin. *C. hystrix* peel essential oil also appears to exhibit anti-inflammatory effects and has potential as an antimelanoma agent. Our data show that CHLE is safe for use on human skin.

4. CONCLUSIONS

We successfully prepared various combinations of composite PVA hydrogels loaded with CHLE, CS, SA, and SA/CS using the freeze−thaw method. Morphological changes in each hydrogel sample, confirmed by SEM images, showed the loading effects of CS, SA, and SA/CS in the PVA/CHLE hydrogel. PVA, CHLE, CS, and SA were contained in the composite hydrogel, as shown in the FTIR spectrum. The XRD characterization showed that the loading of CS, SA, and SA/CS in the PVA/CHLE hydrogel resulted in a decrease in the crystallinity degree. The crystallinity degree obtained from the DSC characterization confirmed the XRD results, while the

https://doi.org/10.1021/acsomega.3c10143
ACS Omega 2024, 9, 13306−13322

TGA characterization showed a decrease in the thermal stability of the PVA/CHLE hydrogel after loading of CS, SA, and SA/CS. The loading of CS, SA, and SA/CS succeeded in reducing the compressive strength of the PVA/CHLE hydrogel so that it was more elastic, which correlated with a decrease in the crystallinity degree. The antibacterial activity of CHLE after being loaded into the composite hydrogel was still maintained, as evidenced by the in vitro antibacterial test. The loading of CS resulted in an increase in antibacterial activity, whereas a decrease in antibacterial activity occurred after the loading of SA. The extract release test proved that the presence of CS, SA, and SA/CS inhibited the release of the extract, resulting in a controlled release following the pseudo-Fickian diffusion. The cytotoxic activity test showed that all hydrogel samples can be used safely on normal cells up to concentrations above 1000 μg/mL.

■ ASSOCIATED CONTENT

Supporting Information

The Supporting Information is available free of charge at https://pubs.acs.org/doi/10.1021/acsomega.3c10143.

Additional graphs for XRD analysis, TGA analysis, thermogram data, inhibition zone results, and cytotoxicity analysis (PDF)

■ AUTHOR INFORMATION

Corresponding Author

Khairurrijal Khairurrijal − *Department of Physics, Faculty of Mathematics and Natural Sciences, Institut Teknologi Bandung, Bandung 40132, Indonesia; University Center of Excellence—Nutraceutical, Bioscience and Biotechnology Research Center, Institut Teknologi Bandung, Bandung 40132, Indonesia; Department of Physics, Faculty of Sciences, Institut Teknologi Sumatera, Lampung 35365, Indonesia;* orcid.org/0000-0002-9452-4192; Email: krijal@itb.ac.id

Authors

Kusjuriansah Kusjuriansah − *Department of Physics, Faculty of Mathematics and Natural Sciences, Institut Teknologi Bandung, Bandung 40132, Indonesia*

Marathur Rodhiyah − *Department of Physics, Faculty of Mathematics and Natural Sciences, Institut Teknologi Bandung, Bandung 40132, Indonesia;* orcid.org/0000-0003-3669-5492

Nabila Asy Syifa − *Doctoral Program of Physics, Faculty of Mathematics and Natural Sciences, Institut Teknologi Bandung, Bandung 40132, Indonesia*

Halida Rahmi Luthfianti − *Doctoral Program of Physics, Faculty of Mathematics and Natural Sciences, Institut Teknologi Bandung, Bandung 40132, Indonesia;* orcid.org/0000-0002-3458-0619

William Xaveriano Waresindo − *Doctoral Program of Physics, Faculty of Mathematics and Natural Sciences, Institut Teknologi Bandung, Bandung 40132, Indonesia;* orcid.org/0000-0003-0028-603X

Dian Ahmad Hapidin − *Department of Physics, Faculty of Mathematics and Natural Sciences, Institut Teknologi Bandung, Bandung 40132, Indonesia*

Tri Suciati − *Department of Pharmaceutics, School of Pharmacy, Institut Teknologi Bandung, Bandung 40132, Indonesia*

Dhewa Edikresnha − *Department of Physics, Faculty of Mathematics and Natural Sciences, Institut Teknologi Bandung, Bandung 40132, Indonesia; University Center of Excellence—Nutraceutical, Bioscience and Biotechnology Research Center, Institut Teknologi Bandung, Bandung 40132, Indonesia;* orcid.org/0000-0001-6203-4343

Complete contact information is available at: https://pubs.acs.org/10.1021/acsomega.3c10143

Author Contributions

K.K. contributed to conceptualization, methodology, writing—original draft, and data curation. M.R. contributed to experiment and analysis. N.A.S., H.R.L., and W.X.W. contributed to conceptualization, methodology, and data curation. D.A.H. contributed to resources and supervision. T.S. contributed to resources and supervision. D.E. contributed to resources, writing—review, editing, supervision, and funding acquisition. K.K. contributed to resources, writing—review, editing, and supervision.

Notes

The authors declare no competing financial interest.

■ ACKNOWLEDGMENTS

This research was financially supported by the Directorate of Research and Community Engagement, Institut Teknologi Bandung, under the "ITB Research Program" (Program Riset ITB) Grant in the fiscal years of 2020−2021 contract number 139/IT1.B07.1/TA.00/2021. Kusjuriansah Kusjuriansah gratefully acknowledges the Indonesian Endowment Fund for Education (LPDP) for the provision of the master scholarship. The authors would also like to thank Basic Science Center A, Faculty of Mathematics and Natural Sciences, ITB, for conducting SEM characterization.

■ REFERENCES

(1) Ulhaq, Z. S.; Hendyatama, T. H.; Hameed, F.; Santosaningsih, D. Antibacterial Activity of Citrus Hystrix toward Salmonella Spp. Infection. *Enferm. Infecc. Microbiol. Clin.* **2021**, *39*, 283−286.

(2) Samraj, S.; Rajamurgugan, S. Qualitative & Quantitative Estimation of Bioactive Compounds and Antioxidant Activity in Citrus Hystrix. *Int. J. Eng. Sci. Comput.* **2017**, *7* (6), 13154−13163.

(3) Srifuengfung, S.; Bunyapraphatsara, N.; Satitpatipan, V.; Tribuddharat, C.; Junyaprasert, V. B.; Tungrugsasut, W.; Srisukh, V. Antibacterial Oral Sprays from Kaffir Lime (Citrus Hystrix DC.) Fruit Peel Oil and Leaf Oil and Their Activities against Respiratory Tract Pathogens. *J. Tradit. Complementary Med.* **2020**, *10*, 594−598.

(4) Srisukh, V.; Tribuddharat, C.; Nukoolkarn, V.; Bunyapraphatsara, N.; Chokephaibulkit, K.; Phoomniyom, S.; Chuanphung, S.; Srifuengfung, S. Antibacterial Activity of Essential Oils from Citrus Hystrix (Makrut Lime) against Respiratory Tract Pathogens. *ScienceAsia* **2012**, *38*, 212−217.

(5) Singh, N.; Agarwal, S.; Jain, A.; Khan, S. 3-Dimensional Cross Linked Hydrophilic Polymeric Network "Hydrogels": An Agriculture Boom. *Agric. Water Manage.* **2021**, *253*, 1−14.

(6) Liu, K.; Chen, Y.; Zha, X.; Li, Q.; Pan, L.; Luo, J. Research Progress on Polysaccharide/Protein Hydrogels : Preparation Method, Functional Property and Application as Delivery Systems for Bioactive Ingredients. *Food Res. Int.* **2021**, *147*, 1−16.

(7) Madduma-bandarage, U. S. K.; Madihally, S. V. Synthetic Hydrogels : Synthesis, Novel Trends, and Applications. *J. Appl. Polym. Sci.* **2020**, *138*, No. 50376.

(8) Popescu, I.; Turtoi, M.; Sufle, D. M.; Dinu, M. V.; Darie-nita, R. N.; Anghelache, M.; Calin, M.; Constantin, M. Alginate/Poloxamer Hydrogel Obtained by Thiol-Acrylate Photopolymerization for the

Alleviation of the Inflammatory Response of Human Keratinocytes. *Int. J. Biol. Macromol.* **2021**, *180*, 418−431.
(9) Kamaci, M.; Kaya, I. Preparation of Biodegradable, and PH-Sensitive Poly(Azomethine)-Chitosan Hydrogels for Potential Application of 5-Fluoro Uracil Delivery. *Eur. Polym. J.* **2021**, *158*, 1−11.
(10) Bashir, S.; Hina, M.; Iqbal, J.; Rajpar, A. H.; Mujtaba, M. A.; Alghamdi, N. A.; Wageh, S.; Ramesh, K.; Ramesh, S. Fundamental Concepts of Hydrogels: Synthesis, Properties, and Their Applications. *Polymers* **2020**, *12*, 1−60.
(11) Asy-Syifa, N.; Waresindo, W. X.; Edikresnha, D.; Suciati, T.; Khairurrijal, K.; et al. The Study of the Swelling Degree of the PVA Hydrogel with Varying Concentrations of PVA. *J. Phys.: Conf. Ser.* **2022**, *2243*, No. 012053.
(12) Rivera-Hernandez, G.; Antunes-Ricardo, M.; Martínez-Morales, P.; Sanchez, M. L. Polyvinyl Alcohol Based-Drug Delivery Systems for Cancer Treatment Gabriela. *Int. J. Pharm.* **2021**, *600*, 1−11.
(13) Marin, E.; Rojas, J.; Ciro, Y. A Review of Polyvinyl Alcohol Derivatives: Promising Materials for Pharmaceutical and Biomedical Applications. *Afr. J. Pharm. Pharmacol.* **2014**, *8*, 674−684.
(14) Zhang, M.; Zhao, X. Alginate Hydrogel Dressings for Advanced Wound Management. *Int. J. Biol. Macromol.* **2020**, *162*, 1414−1428.
(15) Kong, F.; Fan, C.; Yang, Y.; Hoon, B.; Wei, K. 5-Hydroxymethylfurfural-Embedded Poly (Vinyl Alcohol)/Sodium Alginate Hybrid Hydrogels Accelerate Wound Healing. *Int. J. Biol. Macromol.* **2019**, *138*, 933−949.
(16) Peers, S.; Montembault, A.; Ladavière, C. Chitosan Hydrogels for Sustained Drug Delivery. *J. Controlled Release* **2020**, *326*, 150−163.
(17) Zhang, Y.; Jiang, M.; Zhang, Y.; Cao, Q.; Wang, X.; Han, Y.; Sun, G.; Li, Y.; Zhou, J. Novel Lignin−Chitosan−PVA Composite Hydrogel for Wound Dressing. *Mater. Sci. Eng., C* **2019**, *104* (October2018), No. 110002.
(18) Afshar, M.; Dini, G.; Vaezifar, S.; Mehdikhani, M.; Movahedi, B. Preparation and Characterization of Sodium Alginate/Polyvinyl Alcohol Hydrogel Containing Drug-Loaded Chitosan Nanoparticles as a Drug Delivery System. *J. Drug Delivery Sci. Technol.* **2020**, *56*, 1−6.
(19) Ali, A.; Ahmed, S. Recent Advances in Edible Polymer Based Hydrogels as a Sustainable Alternative to Conventional Polymers. *J. Agric. Food Chem.* **2018**, *66*, 6940−6967.
(20) Edikresnha, D.; Suciati, T.; Suprijadi, S.; Khairurrijal, K. Freeze-Thawed Hydrogel Loaded by Piper Crocatum Extract with In-Vitro Antibacterial and Release Tests. *J. Mater. Res. Technol.* **2021**, *15*, 17−36.
(21) Waresindo, W. X.; Luthfianti, H. R.; Edikresnha, D.; Suciati, T.; Noor, F. A.; Khairurrijal, K. A Freeze–Thaw PVA Hydrogel Loaded with Guava Leaf Extract: Physical and Antibacterial Properties. *RSC Adv.* **2021**, *11* (48), 30156−30171.
(22) Koosha, M.; Aalipour, H.; Shirazi, M. J. S.; Jebali, A.; Chi, H.; Hamedi, S.; Wang, N.; Li, T.; Moravvej, H. Physically Crosslinked Chitosan/PVA Hydrogels Containing Honey and Allantoin with Long-Term Biocompatibility for Skin Wound Repair: An In Vitro and In Vivo Study. *J. Funct. Biomater.* **2021**, *12*, 1−19.
(23) Kamoun, E. A.; Kenawy, E.-R. S.; Tamer, T. M.; El-Meligy, M. A.; Eldin, M. S. M. Poly (Vinyl Alcohol)-Alginate Physically Crosslinked Hydrogel Membranes for Wound Dressing Applications: Characterization and Bio-Evaluation. *Arab. J. Chem.* **2015**, *8* (1), 38−47.
(24) Zhang, M.; Wang, G.; Wang, D.; Zheng, Y.; Li, Y.; Meng, W.; Zhang, X.; Du, F.; Lee, S. Ag@MOF-Loaded Chitosan Nanoparticle and Polyvinyl Alcohol/Sodium Alginate/Chitosan Bilayer Dressing for Wound Healing Applications. *Int. J. Biol. Macromol.* **2021**, *175*, 481−494.
(25) Nendissa, S. J.; Nendissa, D. M. Test for the Antibacterial Inhibition of Kaffir Lime Leaf (Citrus Hysteric D.C) Extract against Pathogen Bacteria in Improving Food Safety. *IOP Conf. Ser.: Earth Environ. Sci.* **2021**, *883*, 1−6.
(26) Purnama; Farabi, K.; Runadi, D.; Kuncoro, H.; Harneti, D.; Nurlelasari; Mayanti, T.; Azmi, M. N.; Fajriah, S.; Supratman, U. The Cytotoxic Activity of Dammarane-Type Triterpenoids Isolated from the Stem Bark of Aglaia Cucullata (Meliaceae). *Molecules* **2023**, *28* (13), 1−13.
(27) Gupta, S.; Pramanick, A. K.; Kailath, A.; Delhi, N.; Mishra, T.; et al. Composition Dependent Structural Modulations in Transparent Poly(Vinyl Alcohol) Hydrogels. *Colloids Surf., B* **2009**, *74*, 186−190.
(28) Bialik-Wąs, K.; Pluta, K.; Malina, D.; Barczewski, M.; Malarz, K.; Mrozek-Wilczkiewicz, A. Advanced SA/PVA-Based Hydrogel Matrices with Prolonged Release of Aloe Vera as Promising Wound Dressings. *Mater. Sci. Eng., C* **2021**, *120*, No. 111667.
(29) Menchicchi, B.; Hensel, A.; Goycoolea, F. Polysaccharides as Bacterial Antiadhesive Agents and "Smart" Constituents for Improved Drug Delivery Systems Against Helicobacter Pylori Infection. *Curr. Pharm. Des.* **2015**, *21* (33), 4888−4906.
(30) Jumat, M. A.; Zahidin, N. S.; Zaini, M. A. A.; Fadzil, N. A.; Nur, H.; Saidin, S. Incorporation of Acalypha Indica Extract in Polyvinyl Alcohol Hydrogels: Physico-Chemical, Antibacterial and Cell Compatibility Analyses. *J. Teknol.* **2021**, *83*, 57−65.
(31) Kumar, A.; Behl, T.; Chadha, S. Synthesis of Physically Crosslinked PVA/Chitosan Loaded Silver Nanoparticles Hydrogels with Tunable Mechanical Properties and Antibacterial Effects. *Int. J. Biol. Macromol.* **2020**, *149*, 1262−1274.
(32) Părpăriţă, E.; Cheaburu, C. N.; Paţachia, S. F.; Vasile, C. Polyvinyl Alcohol/Chitosan/Montmorillonite Nanocomposites Preparation by Freeze/Thaw Cycles and Characterization. *Acta Chem. Iasi* **2014**, *22*, 75−96.
(33) Omkaram, I.; Chakradhar, R. P. S.; Rao, J. L. EPR, Optical, Infrared and Raman Studies of VO2+ Ions in Polyvinylalcohol Film. *Phys. B* **2007**, *388*, 318−325.
(34) Bhat, N. V.; Nate, M. M.; Kurup, M. B.; Bambole, V. A.; Sabharwal, S. Effect of Gamma-Radiation on the Structure and Morphology of Polyvinyl Alcohol Films. *Nucl. Instrum. Methods Phys. Res. B* **2005**, *237*, 585−592.
(35) Lazidou, D.; Teknetzi, I.; Karapanagiotis, I.; Ritzoulis, C.; Panayiotou, C. Poly(Vinyl Alcohol)-Borax Films as Cleaning Agents for Icons. *Archaeol. Anthropol. Sci.* **2019**, *11*, 6259−6271.
(36) Azlah, M. A. F.; Chua, L. S.; Abdullah, F. I.; Yam, M. F. A Fast and Reliable 2D-IR Spectroscopic Technique for Herbal Leaves Classification. *Vib. Spectrosc.* **2020**, *106*, 1−7.
(37) Navitania, H.; Tyanti, H. W.; Sukamto. The Atsiri Oil Citrus Hystrix and Cymbopogon Citratus in Caloric Value of Premium. *J. Tek. Kim.* **2019**, *13* (2), 44−48.
(38) Fenoradosoa, T. A.; Ali, G.; Delattre, C.; Laroche, C.; Petit, E.; Wadouachi, A.; Michaud, P. Extraction and Characterization of an Alginate from the Brown Seaweed Sargassum Turbinarioides Grunow. *J. Appl. Phycol.* **2010**, *22*, 131−137.
(39) Maharani, A. A.; Husni, A.; Ekantari, N. Karakteristik Natrium Alginat Rumput Laut Cokelat Sargassum Fluitans Dengan Metode Ekstraksi Yang Berbeda. *JPHPI* **2017**, *20*, 478−487.
(40) Fernandes Queiroz, M.; Melo, K. R. T. M.; Sabry, D. A.; Sassaki, G. L.; Rocha, H. A. O. Does the Use of Chitosan Contribute to Oxalate Kidney Stone Formation? *Mar. Drugs* **2015**, *13*, 141−158.
(41) Piasecka-zelga, J.; Zelga, P.; Szulc, J.; Wietecha, J.; Ciecha, D. An in Vivo Biocompatibility Study Ofsurgical Meshes Made from Bacterial Cellulose Modified with Chitosan. *Int. J. Biol. Macromol.* **2018**, *116*, 1119−1127.
(42) Choo, K.; Ching, Y. C.; Chuah, C. H.; Julai, S.; Liou, N. S. Preparation and Characterization of Polyvinyl Alcohol-Chitosan Composite Films Reinforced with Cellulose Nanofiber. *Materials* **2016**, *9*, 1−16.
(43) Aziz, S. B.; Marf, A. S.; Dannoun, E. M. A.; Brza, M. A.; Abdullah, R. M. The Study of the Degree of Crystallinity, Electrical Equivalent Circuit, and Dielectric Properties of Polyvinyl Alcohol (PVA)-Based Biopolymer Electrolytes. *Polymers* **2020**, *12* (10), No. 2184.

https://doi.org/10.1021/acsomega.3c10143
ACS Omega 2024, 9, 13306−13322

(44) Aziz, S. B.; Abdulwahid, R. T.; Rasheed, M. A.; Abdullah, O. G.; Ahmed, H. M. Polymer Blending as a Novel Approach for Tuning the SPR Peaks of Silver Nanoparticles. *Polymers* **2017**, *9*, 1−12.
(45) Aziz, S. B.; Abdullah, O. G.; Rasheed, M. A.; Ahmed, H. M. Effect of High Salt Concentration (HSC) on Structural, Morphological, and Electrical Characteristics of Chitosan Based Solid Polymer Electrolytes. *Polymers* **2017**, *9*, 1−19.
(46) Ioelovich, M. Crystallinity and Hydrophility of Chitin and Chitosan. *Res. Rev. J. Chem.* **2014**, *3*, 7−14.
(47) Shameem, A.; Devendran, P.; Siva, V.; Venkatesh, K. S.; Manikandan, A.; Bahadur, S. A.; Nallamuthu, N. Dielectric Investigation of NaLiS Nanoparticles Loaded on Alginate Polymer Matrix Synthesized by Single Pot Microwave Irradiation. *J. Inorg. Organomet. Polym. Mater.* **2018**, *28*, 671−678.
(48) Sundarrajan, P.; Eswaran, P.; Marimuthu, A.; et al. One Pot Synthesis and Characterization of Alginate Stabilized Semiconductor Nanoparticles. *Bull. Korean Chem. Soc.* **2012**, *33*, 1−8.
(49) Helmiyati; Aprilliza, M. Characterization and Properties of Sodium Alginate from Brown Algae Used as an Ecofriendly Superabsorbent. *IOP Conf. Ser.: Mater. Sci. Eng.* **2017**, *188*, 1−5.
(50) Menazea, A. A.; Ismail, A. M.; Awwad, N. S.; Ibrahium, H. A. Physical Characterization and Antibacterial Activity of PVA/Chitosan Matrix Doped by Selenium Nanoparticles Prepared via One-Pot Laser Ablation Route. *J. Mater. Res. Technol.* **2020**, *9*, 9598−9606.
(51) Eghbalifam, N.; Frounchi, M.; Dadbin, S. Antibacterial Silver Nanoparticles in Polyvinyl Alcohol/Sodium Alginate Blend Produced by Gamma Irradiation. *Int. J. Biol. Macromol.* **2015**, *80*, 170−176.
(52) Zhao, X.; Wang, X.; Lou, T. Preparation of Fibrous Chitosan/Sodium Alginate Composite Foams for the Adsorption of Cationic and Anionic Dyes. *J. Hazard. Mater.* **2021**, *403*, 1−10.
(53) Kenawy, E.-R.; Kamoun, E. A.; El-meligy, M. A.; Eldin, M. S. M. Physically Crosslinked Poly(Vinyl Alcohol)-Hydroxyethyl Starch Blend Hydrogel Membranes: Synthesis and Characterization for Biomedical Applications. *Arab. J. Chem.* **2014**, *7*, 372−380.
(54) Yang, J. M.; Wang, H. Z.; Yang, C. C. Modification and Characterization of Semi-Crystalline Poly(Vinyl Alcohol) with Interpenetrating Poly(Acrylic Acid) by UV Radiation Method for Alkaline Solid Polymer Electrolytes Membrane. *J. Membr. Sci.* **2008**, *322*, 74−80.
(55) Holland, B. J.; Hay, J. N. The Thermal Degradation of Poly(Vinyl Alcohol). *Polymer* **2001**, *42*, 6775−6783.
(56) Reguieg, F.; Ricci, L.; Bouyacoub, N.; Belbachir, M.; Bertoldo, M. Thermal Characterization by DSC and TGA Analyses of PVA Hydrogels with Organic and Sodium MMT. *Polym. Bull.* **2020**, *77* (2), 929−948.
(57) Park, H.; Kwon, O.; Ryu, K. Thermal Stability and Degradation Kinetics of Polyphenols and Polyphenylenediamines Enzymatically Synthesized by Horseradish Peroxidase. *Korean J. Chem. Eng.* **2015**, *32*, 1847−1852.
(58) Beck, M.; Winterhalter, R.; Herrmann, F.; Moortgat, G. K. The Gas-Phase Ozonolysis of a-Humulene. *Phys. Chem. Chem. Phys.* **2011**, *13*, 10970−11001.
(59) El Asbahani, A.; Miladi, K.; Badri, W.; Sala, M.; Addi, E. H. A.; Casabianca, H.; El Mousadik, A.; Hartmann, D.; Jilale, A.; Renaud, F. N. R.; Elaissari, A. Essential Oils: From Extraction to Encapsulation. *Int. J. Pharm.* **2015**, *483*, 220−243.
(60) Chan, W. K.; Tan, L. T. H.; Chan, K. G.; Lee, L. H.; Goh, B. H. Nerolidol: A Sesquiterpene Alcohol with Multi-Faceted Pharmacological and Biological Activities. *Molecules* **2016**, *21*, No. 529, DOI: 10.3390/molecules21050529.
(61) Biranje, S.; Madiwale, P.; Adivarekar, R. V. Preparation and Characterization of Chitosan/PVA Polymeric Film for Its Potential Application as Wound Dressing Material. *Indian J. Sci. Res.* **2017**, *14*, 250−256.
(62) Kumar, D.; Raj, V.; Verma, A.; Kumar, P.; Pandey, J. Novel Binary Grafted Chitosan Nanocarrier for Sustained Release of Curcumin. *Int. J. Biol. Macromol.* **2019**, *131*, 184−191.
(63) Flores-Hernández, C. G.; Cornejo-villegas, M. D. L.; Moreno-martell, A.; Real, A. D. Synthesis of a Biodegradable Polymer of Poly (Sodium Alginate/Ethyl Acrylate). *Polymers* **2021**, *13*, 1−12.
(64) Baigorria, E.; Cano, L. A.; Sanchez, L. M.; Alvarez, V. A.; Ollier, R. P. Bentonite-Composite Polyvinyl Alcohol/Alginate Hydrogel Beads: Preparation, Characterization and Their Use as Arsenic Removal Devices. *Environ. Nanotechnol., Monit. Manage.* **2020**, *14*, 1−8.
(65) Sung, J. H.; Hwang, M.; Kim, J. O.; Lee, J. H.; Kim, Y. Il.; Kim, J. H.; Chang, S. W.; Jin, G. S.; Kim, J.; Loo, S. W.; Han, S. S.; Ku, S. K.; Yong, S. C.; Choi, H. Gel Characterisation and in Vivo Evaluation of Minocycline-Loaded Wound Dressing with Enhanced Wound Healing Using Polyvinyl Alcohol and Chitosan. *Int. J. Pharm.* **2010**, *392*, 232−240.
(66) Lei, Q.; Zhang, Y.; Zhang, W.; Li, R.; Ao, N.; Zhang, H. A Synergy between Dopamine and Electrostatically Bound Bactericide in a Poly (Vinyl Alcohol) Hybrid Hydrogel for Treating Infected Wounds. *Carbohydr. Polym.* **2021**, *272*, 1−12.
(67) Koyano, T.; Koshizaki, N.; Umehara, H.; Nagura, M.; Minoura, N. Surface States of PVA/Chitosan Blended Hydrogels. *Polymer* **2000**, *41*, 4461−4465.
(68) Luthfianti, H. R.; Waresindo, W. X.; Edikresnha, D.; Chahyadi, A.; Suciati, T.; Noor, F. A.; Khairurrijal, K. Physicochemical Characteristics and Antibacterial Activities of Freeze-Thawed Polyvinyl Alcohol/Andrographolide Hydrogels. *ACS Omega* **2023**, *8* (3), 2915−2930.
(69) Mukherjee, D.; Azamthulla, M.; Santhosh, S.; Dath, G.; Ghosh, A.; et al. Development and Characterization of Chitosan-Based Hydrogels as Wound Dressing Materials. *J. Drug Delivery Sci. Technol.* **2018**, *46*, 498−510.
(70) Waresindo, W. X.; Luthfianti, H. R.; Priyanto, A.; Hapidin, D. A.; Edikresnha, D.; Aimon, A. H.; Suciati, T.; Khairurrijal, K. Freeze-Thaw Hydrogel Fabrication Method: Basic Principles, Synthesis Parameters, Properties, and Biomedical Applications. *Mater. Res. Express* **2023**, *10* (2), No. 024003.
(71) Indiarto, R.; Nurhadi, B.; Subroto, E. Study of Characteristics Texture (Texture Profile Analysis) and Organoleptic Smoked Chicken Based on Liquid Smoke Technology from Coconut Shell. *J. Teknol. Has. Pertan.* **2012**, *V* (2), 106−116.
(72) Cheaburu-yilmaz, C. N.; Yilmaz, O.; Kose, F. A.; Bibire, N. Chitosan-Graft-Poly (N-Isopropylacrylamide)/PVA Cryogels as Carriers for Mucosal Delivery of Voriconazole. *Polymers* **2019**, *11* (1432), 1−20.
(73) Gupta, S.; Webster, T. J.; Sinha, A. Evolution of PVA Gels Prepared without Crosslinking Agents as a Cell Adhesive Surface. *J. Mater. Sci.: Mater. Med.* **2011**, *22* (7), 1763−1772.
(74) Yang, X.; Liu, Q.; Chen, X.; Yu, F.; Zhu, Z. Investigation of PVA/Ws-Chitosan Hydrogels Prepared by Combined Gamma-Irradiation and Freeze-Thawing. *Carbohydr. Polym.* **2008**, *73*, 401−408.
(75) Kamoun, E. A.; Chen, X.; Eldin, M. S. M.; Kenawy, E.-R. S. Crosslinked Poly (Vinyl Alcohol) Hydrogels for Wound Dressing Applications: A Review of Remarkably Blended Polymers. *Arab. J. Chem.* **2015**, *8* (1), 1−14.
(76) Liu, Q.; Li, Q.; Xu, S.; Zheng, Q.; Cao, X. Preparation and Properties of 3D Printed Alginate−Chitosan Polyion Complex Hydrogels for Tissue Engineering. *Polymers* **2018**, *10* (6), No. 664.
(77) Wang, Y. J.; Zhang, X. N.; Song, Y.; Zhao, Y.; Chen, L.; Su, F.; Li, L.; Wu, Z. L.; Zheng, Q. Ultrastiff and Tough Supramolecular Hydrogels with a Dense and Robust Hydrogen Bond Network. *Chem. Mater.* **2019**, *31* (4), 1430−1440.
(78) Edikresnha, D.; Suciati, T.; Munir, M. M.; Khairurrijal, K. Polyvinylpyrrolidone/Cellulose Acetate Electrospun Composite Nanofibres Loaded by Glycerine and Garlic Extract with: In Vitro Antibacterial Activity and Release Behaviour Test. *RSC Adv.* **2019**, *9* (45), 26351−26363.
(79) Bernal-Ballen, A.; Lopez-Garcia, J.; Merchan-Merchan, M. A.; Lehocky, M. Synthesis and Characterization of a Bioartificial

Polymeric System with Potential Antibacterial Activity: Chitosan-Polyvinyl Alcohol-Ampicillin. *Molecules* **2018**, *28* (12), No. 3109.
(80) Lopez-Romero, J. C.; González-Ríos, H.; Borges, A.; Simões, M. Antibacterial Effects and Mode of Action of Selected Essential Oils Components against *Escherichia Coli* and Staphylococcus Aureus. *Evidence-Based Complementary Altern. Med.* **2015**, *2015*, 1−9.
(81) Atay, H. Y. Antibacterial Activity of Chitosan-Based Systems. *Funct. Chitosan* **2020**, 457−489.
(82) Chen, J.; Wu, A.; Yang, M.; Ge, Y.; Pristijono, P.; Li, J.; Xu, B.; Mi, H. Characterization of Sodium Alginate-Based Films Incorporated with Thymol for Fresh-Cut Apple Packaging. *Food Control* **2021**, *126*, 1−8.
(83) Tahtat, D.; Mahlous, M.; Benamer, S.; Nacer Khodja, A.; Larbi Youcef, S.; Hadjarab, N.; Mezaache, W. Influence of Some Factors Affecting Antibacterial Activity of PVA/Chitosan Based Hydrogels Synthesized by Gamma Irradiation. *J. Mater. Sci.: Mater. Med.* **2011**, *22*, 2505.
(84) Huang, X.; Brazel, C. S. On the Importance and Mechanisms of Burst Release in Matrix-Controlled Drug Delivery Systems. *J. Controlled Release* **2001**, *73*, 121.
(85) Hadjianfar, M.; Semnani, D.; Varshosaz, J. Polycaprolactone/Chitosan Blend Nanofibers Loaded by 5-fluorouracil: An Approach to Anticancer Drug Delivery System. *Polym. Adv. Technol.* **2018**, *29*, 1−10.
(86) Chopra, H.; Bibi, S.; Kumar, S.; Khan, M. S.; Kumar, P.; Singh, I. Preparation and Evaluation of Chitosan/PVA Based Hydrogel Films Loaded with Honey for Wound Healing Application. *Gels* **2022**, *8* (111), 1−21.
(87) Tønnesen, H. H.; Karlsen, J. Alginate in Drug Delivery Systems. *Drug Dev. Ind. Pharm.* **2002**, *28* (6), 621−630.
(88) Siti, H. N.; Mohamed, S.; Kamisah, Y. Potential Therapeutic Effects of Citrus Hystrix DC and Its Bioactive Compounds on Metabolic Disorders. *Pharmaceuticals* **2022**, *15* (167), 1−21.
(89) Tchaikovskaya, O. N.; Basyl, O. K.; Sultimova, N. B. Proton-Acceptor and Proton-Donor Properties of Phenol and Its Substitutes. *Russ. Phys. J.* **2005**, *48* (12), 1245−1250.
(90) Meng, X.; Tian, F.; Yang, J.; He, C.-N.; Xing, N.; Li, F. Chitosan and Alginate Polyelectrolyte Complex Membranes and Their Properties for Wound Dressing Application. *J. Mater. Sci.: Mater. Med.* **2010**, *21*, 1751−1759.
(91) Sánchez-Aguinagalde, O.; Lejardi, A.; Meaurio, E.; Hernández, R.; Mijangos, C.; Sarasua, J. Novel Hydrogels of Chitosan and Poly(Vinyl Alcohol) Reinforced with Inorganic Particles of Bioactive Glass. *Polymers* **2021**, *13* (691), 1−14.
(92) Das, S.; Subuddhi, U. Controlled Delivery of Ibuprofen from Poly(Vinyl Alcohol)?Poly (Ethylene Glycol) Interpenetrating Polymeric Network Hydrogels. *J. Pharm. Anal.* **2019**, *9* (2), 108−116.
(93) Gull, N.; Taqi, M.; Butt, Z.; Zia, S.; Khan, R. U.; King, M. W. Hybrid Cross-linked Hydrogels as a Technology Platform for in Vitro Release of Cephradine. *Polym. Adv. Technol.* **2019**, 1−11.
(94) Kim, T.; Seol, D. R.; Hahm, S.; Ko, C.; Kim, E.; Chun, K.; Kim, J.; Lim, T. Analgesic Effect of Intra-Articular Injection of Temperature-Responsive Hydrogel Containing Bupivacaine on Osteoarthritic Pain in Rats. *Biomed. Res. Int.* **2015**, *2015*, 1−9.
(95) Lall, N.; Henley-smith, C. J.; Canha, M. N. D.; Oosthuizen, C. B.; Berrington, D. Viability Reagent, PrestoBlue, in Comparison with Other Available Reagents, Utilized in Cytotoxicity and Antimicrobial Assays. *Int. J. Microbiol.* **2013**, *2013*, 1−5.
(96) Sianipar, N. F.; Hadisaputri, Y. E.; Assidqi, K.; Simanjuntak, P.; Purnamaningsih, R. A Study of Anticancer Activity from the Fractions of Rodent Tuber Superior Mutant Extract (Typhonium Flagelliforme) by Prestoblue Assay Method. *Rasayan J. Chem.* **2020**, *13* (3), 1992−1998.
(97) Varçin, M.; Şener, B. B.; Bayraç, C. Adsorption of Resazurin by Poly(Acrylic Acid) Hydrogels and Evaluation of Its Use in Reduction Assay for Quantification of Cell Viability. *Dyes Pigm.* **2021**, *186* (November), No. 109038.
(98) Abyar, S.; Khandar, A. A.; Salehi, R.; Abolfazl Hosseini-Yazdi, S.; Alizadeh, E.; Mahkam, M.; Jamalpoor, A.; White, J. M.; Shojaei, M.; Aizpurua-Olaizola, O.; Masereeuw, R.; Janssen, M. J. In Vitro Nephrotoxicity and Anticancer Potency of Newly Synthesized Cadmium Complexes. *Sci. Rep.* **2019**, *9* (1), No. 14686.
(99) Kulig, M.; Galanty, A.; Grabowska, K.; Podolak, I. Assessment of Safety and Health-Benefits of Citrus Hystrix DC. Peel Essential Oil, with Regard to Its Bioactive Constituents in an in Vitro Model of Physiological and Pathological Skin Conditions. *Biomed. Pharmacother.* **2022**, *151* (May), No. 113151.

https://doi.org/10.1021/acsomega.3c10143
ACS Omega 2024, 9, 13306−13322